Inorganic Chemistry

Article

pubs.acs.org/IC

Synthesis, Characterization, and Spectroscopic Investigation of New Iron(III) and Copper(II) Complexes of a Carboxylate Rich Ligand and Their Interaction with Carbohydrates in Aqueous Solution

Christopher D. Stewart, Hadi Arman, Huda Bawazir, and Ghezai T. Musie*

Department of Chemistry, The University of Texas at San Antonio, San Antonio, Texas 78249, United States

Supporting Information

ABSTRACT: New tetra-iron(III) ($K_4[\mathbf{1}]\cdot 25H_2O\cdot(CH_3)_2CO$ and $K_3[\mathbf{2}]\cdot 3H_2O\cdot(OH)$) and di-copper(II) ($Na_3[\mathbf{3}]\cdot 5H_2O$) complexes as carbohydrate binding models have been synthesized and fully characterized used several techniques including single crystal X-ray crystallography. Whereas $K_4[\mathbf{1}]\cdot 25H_2O\cdot(CH_3)_2CO$ and $Na_3[\mathbf{3}]\cdot 5H_2O$ are completely water-soluble, $K_3[\mathbf{2}]\cdot 3H_2O\cdot(OH)$ is less soluble in all common solvents including water. The binding of substrates, such as D-mannose, D-glucose, D-xylose, and xylitol with the water-soluble complexes in different reaction conditions were investigated. In aqueous alkaline media, complexes $K_4[\mathbf{1}]\cdot 25H_2O\cdot(CH_3)_2CO$ and $Na_3[\mathbf{3}]\cdot 5H_2O$ showed coordination ability toward the applied substrates. Even in the presence of stoichiometric excess of the substrates, the complexes form only 1:1 (complex/substrate) molar ratio species in solution. Apparent binding constants, pK_{app}, values between the complexes and the substrates were determined and specific mode of substrate binding is proposed. The pK_{app} values showed that D-mannose coordinates strongest to $K_4[\mathbf{1}]\cdot 25H_2O\cdot(CH_3)_2CO$ and $Na_3[\mathbf{3}]\cdot 5H_2O$. Syntheses, characterizations and detailed substrate binding study using spectroscopic techniques and single crystal X-ray diffraction are reported.

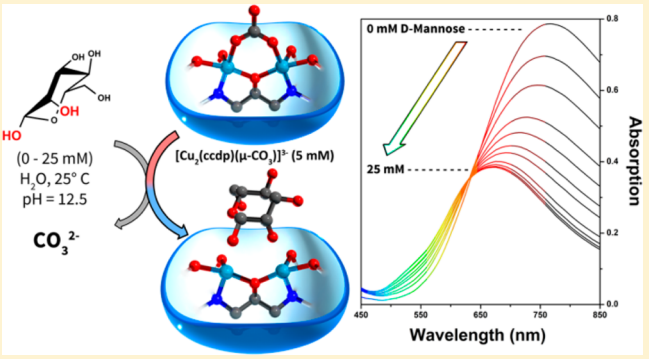

INTRODUCTION

Carbohydrates play several roles in biological functions. Recently, considerable effort has been directed toward understanding carbohydrate recognition, by synthetic receptors, in relation to the important roles that carbohydrates play in biological processes.[1,2] One such recognition which is being investigated with ever increasing interest involves metal ions and carbohydrates interaction.[3−10] This particular interaction has important implications in a variety of biological systems such as support in membrane systems, cell−cell adhesion,[11,12] intercellular recognition, signal transduction, fertilization, and as targets of bacterial or viral infections of cells.[1,2,13] Although understanding the metal ion carbohydrate coordination chemistry is of fundamental importance to these systems, structural and functional investigations of carbohydrate metal complexes has been limited to complexes derived from amino sugars.[14−16] Besides to the biological relevance, carbohydrate interaction with metal ions has also been a subject of intense research in the field of enantioselective catalysis of organic reactions.[17−24]

To understand the carbohydrate metal ion interactions in biological processes, several synthetic complexes have been prepared and reported in the literature as structural and functional models.[25−28] It has also been elucidated that carboxylate-bridged divalent dinuclear complexes with Mg^{2+},[29] Mn^{2+},[30] Co^{2+},[31−34] Ni^{2+},[35] and Zn^{2+}[31,36,37] are involved in many enzymatic nonredox active processes. However, unlike the case with various other metalloenzymes, the study of metalloenzymes involved with carbohydrates using synthetic models is largely unexplored. In the past several years, few research groups have contributed to the understanding of carbohydrate-transition metal ion interactions in chemistry and biology.[12,14−16,24,38−41] For example, synthetic strategies have been developed for VO^{2+},[14] Cr^{3+},[14,41] Mn^{2+},[14] Fe^{3+},[28,42,43] Co^{2+},[31] Ni^{2+},[40] Cu^{2+},[4,7−10] Zn^{2+},[3,31] and MoO_2^{2+} carbohydrate complexes.[40] Furthermore, the biologically relevant aspects of carbohydrate complexes of Fe^{3+},[42,44−47] Cr^{3+},[41] VO^{2+},[48,49] and Zn^{2+},[31,50] have also been studied.

The focus of this paper is on the interaction of monosaccharides with new iron(III) and reported copper(II) complexes of a carboxylate rich dinucleating ligand, *N,N′*-Bis[2-carboxybenzomethyl]-*N,N′*-Bis[carboxymethyl]-1,3-diamino-propan-2-ol (H_5ccdp), Scheme 1, in alkaline aqueous solutions.[51] The synthesis of our H_5ccdp ligand and its derivatives under various reaction conditions is reported elsewhere.[31,51−54] Presently, we report the synthesis and characterization of new tetra-iron(III) complexes ($K_4[\mathbf{1}]\cdot 25H_2O\cdot(CH_3)_2CO$ and $K_3[\mathbf{2}]\cdot 3H_2O\cdot(OH)$) and the di-copper-(II) ($Na_3[\mathbf{3}]\cdot 5H_2O$) complex and their solution interactions

Received: June 13, 2014
Published: October 9, 2014

   dx.doi.org/10.1021/ic501351a | *Inorg. Chem.* 2014, 53, 10974−10988

Scheme 1. Schematic Description of the Synthesis Procedure for $K_4[1]\cdot 25H_2O\cdot(CH_3)_2CO$, $K_3[2]\cdot 3H_2O\cdot(OH)$, and $Na_3[3]\cdot 5H_2O$

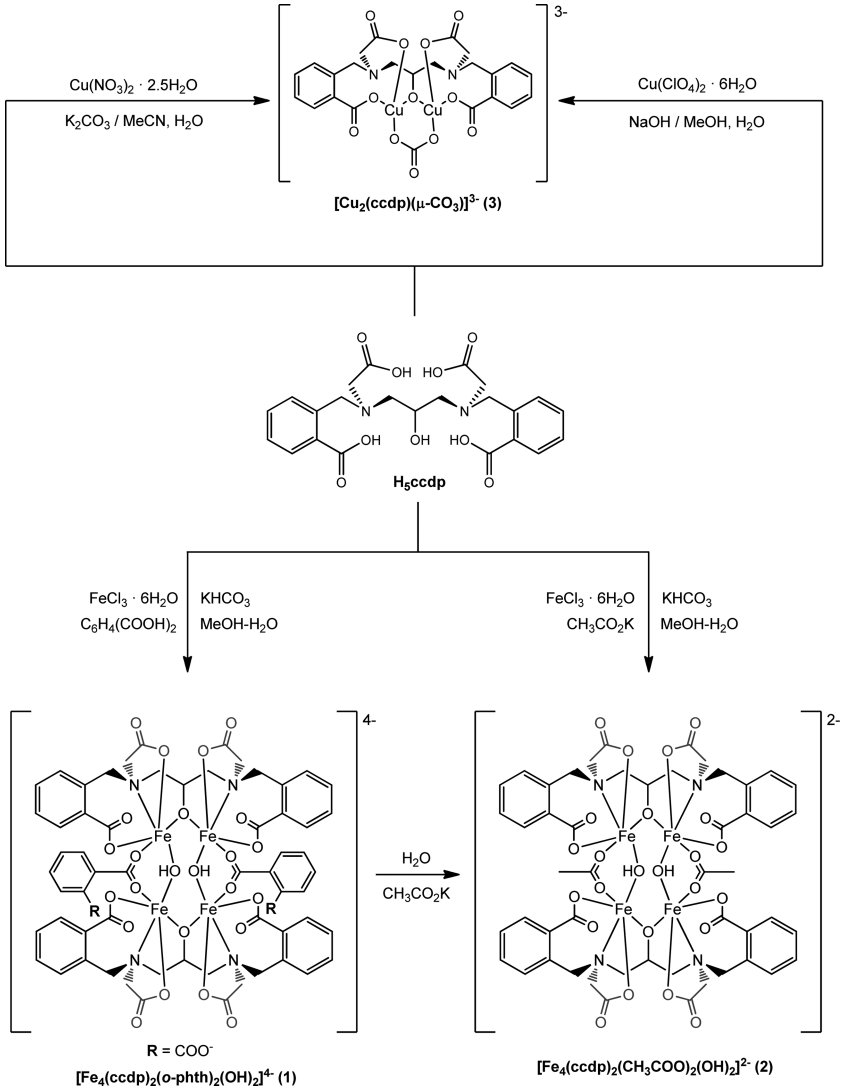

with different physiologically important substrates, D -glucose, D-xylose, and D-mannose. Furthermore, since appreciable amounts of open ring forms of the carbohydrates is generally unattainable in aqueous solutions, the polyalcohol, xylitol, is used as an open ring model for the sugars in the investigation.

RESULTS AND DISCUSSION

Synthesis of the Metal Complexes. The symmetric carboxylate rich dinucleating ligand, H_5ccdp, with central pendant alcoholic arm has been synthesized according to our previously published procedure.[51] The ligand is fully characterized using various analytical techniques such as elemental analysis, FTIR, ^{1}H and ^{13}C NMR spectroscopic analyses. The ligand was selected for this investigation due its carboxylate rich coordination environments, features similar to the structural aspects of the active site of several sugar-metabolizing metalloenzymes, such as Xylose/Glucose Isomerases.[55−57] The direct route to the synthesis of $K_4[1]\cdot 25H_2O\cdot(CH_3)_2CO$, $K_3[2]\cdot 3H_2O\cdot(OH)$ and $Na_3[3]\cdot 5H_2O$ are described in Scheme 1. The reaction of $FeCl_3\cdot 6H_2O$ with the H_5ccdp and phthalic acid in 2:1:1 molar ratio, respectively, in the presence of excess amounts of a mild base, $KHCO_3$, in methanol:H_2O (3:1 by vol.) under refluxing conditions followed by cooling the reaction mixture to room temperature produced a green precipitate of $K_4[1]\cdot 25H_2O\cdot(CH_3)_2CO$. The product is stable and soluble in most common solvents including water. X-ray quality single crystals of $K_4[1]\cdot 25H_2O\cdot(CH_3)_2CO$ were grown by slow acetone diffusion into an aqueous solution of the complex. $K_3[2]\cdot 3H_2O\cdot(OH)$ was synthesized in a very similar fashion except the phthalic acid was replaced with potassium acetate as a reagent in the reaction. However, $K_3[2]\cdot 3H_2O\cdot(OH)$ was produced as a yellow-green precipitate and is insoluble in most common solvents but has very limited solubility in water. Alternatively, a reaction of $K_4[1]\cdot 25H_2O\cdot(CH_3)_2CO$ with stoichiometric excess of potassium acetate in aqueous solution yielded $K_3[2]\cdot 3H_2O\cdot(OH)$ as well, Scheme 1. X-ray quality single crystals of $K_3[2]\cdot 3H_2O\cdot(OH)$ were also grown by slow acetone diffusion into a very dilute aqueous solution of the complex. The $Na_3[3]\cdot 5H_2O$ complex was prepared according to our published procedure.[58] The synthesis and full characterization of the complex has been discussed in the report.[58] Characterization of $K_4[1]\cdot 25H_2O\cdot(CH_3)_2CO$, $K_3[2]\cdot 3H_2O\cdot(OH)$, and $Na_3[3]\cdot 5H_2O$ have been determined using techniques such as elemental analysis, UV−

dx.doi.org/10.1021/ic501351a | Inorg. Chem. 2014, 53, 10974−10988

Table 1. Crystal Data and Structure Refinement for $K_4[1]\cdot 25H_2O\cdot(CH_3)_2CO$, $K_3[2]\cdot 3H_2O\cdot(OH)$, and $Na_3[3]\cdot 5H_2O$[a]

	$K_4[1]\cdot 25H_2O\cdot(CH_3)_2CO$	$K_3[2]\cdot 3H_2O\cdot(OH)$	$Na_3[3]\cdot 5H_2O$
empirical formula	$C_{127}H_{106}N_8O_{88.4}K_{11}Fe_8$	$C_{50}H_{49}N_4O_{30}K_3Fe_4$	$Na_3Cu_2O_{17}N_2C_{24}H_{31}$
formula weight	4035.5	1526.6	801.54
crystal system	triclinic	monoclinic	Monoclinic
space group	$P\bar{1}$	$P2_1/m$	$P2_1/c$
a (Å)	11.4695(5)	11.2843(8)	18.322(3)
b (Å)	16.8686(8)	25.6605(18)	7.4425(10)
c (Å)	22.9044(16)	11.7228(8)	23.236(4)
α (deg)	95.884(7)	90.00	90
β (deg)	103.814(7)	118.009(9)	111.293(2)
γ (deg)	96.178(7)	90.00	90
vol (Å^3)	4240.36	2996.88	2952.2(8)
Z	1	2	4,1
D_{cacld} (g/cm^3)	1.580	1.692	1.803
$\mu(M_o\ K_\alpha)$ (mm^{-1})	1.038	1.253	1.568
$F(000)$	2048	1556	1632
2θ range for data collection (deg)	3.18 to 25.50	3.09 to 27.5	2.44 to 27.50
index ranges	$-10\leq h\geq 13$	$-13\leq h\geq 13$	$-12\leq h\geq 12$
	$-20\leq k\geq 20$	$-30\leq k\geq 30$	$-15\leq k\geq 15$
	$-27\leq l\geq 27$	$-14\leq l\geq 12$	$-14\leq l\geq 12$
reflns collected	26293	17770	21720
ind. reflns	15663 [R_{int} = 0.0265]	5708 [R_{int} = 0.0597]	6764 [R_{int} = 0.0285]
max. and min. transmission	1.000, 0.707	1.000, 0.613	1.000, 0.792
data/restraints/params	15663/1159/0	5708/442/1	6746/0/457
wR (F^2 all data)	R1 = 0.0793	R1 = 0.0771	R1 = 0.0312
	wR2 = 0.1540	wR2 = 0.1413	wR2 = 0.0722
R (F obsd data) [$I > 2\sigma(I)$]	R1 = 0.0668	R1 = 0.0580	R1 = 0.0312
	wR2 = 0.1481	wR2 = 0.1330	wR2 = 0.0846
GOF on F^2	1.116	1.034	1.019
largest diff. peak and hole, e Å^{-3}	2.38/−3.26	0.83/−0.73	0.904/−0.429

[a] wR2 = $\{\Sigma[w[F_0^2 - F_c^2)^2]/\Sigma[w(F_0^2)^2]\}^{1/2}$, R1 = $\Sigma||F_0| - |F_c||/\Sigma|F_0|$.

vis, FTIR, room temperature magnetic measurements, and single-crystal X-ray diffraction.

Spectroscopic Characterization. The UV−vis spectra of 0.01 mM and 0.74 mM concentrations of $K_4[1]\cdot 25H_2O\cdot(CH_3)_2CO$ were recorded in H_2O at pH = 10. The spectrum of low concentration of the yellow solution revealed several features in the UV region corresponding to ligand-to-metal charge transfer (LMCT) transitions. A spectrum with increased concentration by more than order of magnitude revealed two d−d transition bands with λ_{max} centered at 477 and 600 nm, Supporting Information Figure S1. The UV-spectrum of $K_3[2]\cdot 3H_2O\cdot(OH)$ is very similar to that of $K_4[1]\cdot 25H_2O\cdot(CH_3)_2CO$. However, because of its poor solubility, the concentration could not be increased any further to determine features in the visible region, Supporting Information Figure S2. The UV−vis spectra of $Na_3[3]\cdot 5H_2O$ in water has only one d −d transition band λ_{max} centered at 768 nm.

The FT-IR spectra of solid samples of complexes were recorded and analyzed, Supporting Information Figures S3 and S4. The spectra for $K_4[1]\cdot 25H_2O\cdot(CH_3)_2CO$ and $K_3[2]\cdot 3H_2O\cdot(OH)$ possess important common features. For example, the ν_s (Fe−OH−Fe) and ν_{as} (Fe−OH−Fe) vibrational frequencies for the complexes are observed at 663 and 758 cm^{-1}, respectively. The energies of the two vibrations are in agreement with values reported in the literature for similar complexes that hold a Fe−OH−Fe bond angle of 139°.[59] Deacon and Phillips have examined the FT-IR spectra of many metal-carboxylate complexes with known X-ray crystal structures and drawn useful conclusions for the correlations between carboxylate stretching frequencies and their geometries.[60] For example, in the FT-IR spectra of $K_4[1]\cdot 25H_2O\cdot(CH_3)_2CO$, two strong asymmetric $\nu_{as}(COO^-)$ vibrations at 1613 and 1538 cm^{-1} and two strong symmetric $\nu_s(COO^-)$ vibrations were observed at 1365 and 1339 cm^{-1}. The significantly higher difference, Δ ($\Delta = \nu_{as}(COO^-) - \nu_s(COO^-)$) of ∼248 cm^{-1} between the asymmetric and symmetric stretching vibrations is attributed to the monodentate bridging coordination of carboxylate.[60,61] The lower value of Δ at ∼199 cm^{-1} between the asymmetric and symmetric stretching vibrations is indicated by the syn−syn bidentate bridging of the carboxylate.[60,61] The $\nu_{as}(COO^-)$ and $\nu_s(COO^-)$ stretching frequencies of the free carboxylates of the phthalate ligands were assigned to 1571 and 1400 cm^{-1} respectively with a Δ ($\Delta = \nu_{as}(COO^-) - \nu_s(COO^-)$) of 171 cm^{-1}.[60] The analysis of the FT-IR spectrum of $K_3[2]\cdot 3H_2O\cdot(OH)$ was similar to that of $K_4[1]\cdot 25H_2O\cdot(CH_3)_2CO$.

The molar magnetic susceptibility (χ_m) of $K_4[1]\cdot 25H_2O\cdot(CH_3)_2CO$ was calculated at 1.1197×10^{-2} from which the appropriate corrections (Pascal's constants) were applied to obtain a value for χ_A of 1.0283×10^{-2}. The magnetic moment of 4.93 μ_B/Fe$_4$ at T = 296 K for $K_4[1]\cdot 25H_2O\cdot(CH_3)_2CO$ was then determined by Guoy methods.[62,63] This value is comparable to those reported for similar complexes with μ−OH and bridging acetate moieties[64−70] and significantly smaller than the spin-only magnetic moment ($\mu_S = g[ZS(S+1)]^{1/2}$, g = 2, S = 5/2, Z = 4] of 11.83 μ_B/Fe$_4$) expected for four independent high-spin Fe(III) ions, indicating antiferromagnetic nature of interaction between the Fe(III) sites. The

dx.doi.org/10.1021/ic501351a | Inorg. Chem. 2014, 53, 10974−10988

Table 2. Selected Bond Lengths and Angles in $K_4[1]\cdot 25H_2O\cdot(CH_3)_2CO$, $K_3[2]\cdot 3H_2O\cdot(OH)$, and $Na_3[3]\cdot 5H_2O$

bond lengths [Å]					
$K_4[1]\cdot 25H_2O\cdot(CH_3)_2CO$		$K_3[2]\cdot 3H_2O\cdot(OH)$		$Na_3[3]\cdot 5H_2O$	
Fe(1)−O(1)	1.988(3)	Fe(1)−O(8)	2.045(3)	Cu(1)−O(1)	1.982(2)
Fe(1)−O(22)	2.047(4)	Fe(1)−O(10)	2.043(3)	Cu(1)−O(5)	1.913(2)
Fe(1)−O(5)	2.023(4)	Fe(1)−O(11)	2.040(3)	Cu(1)−O(10)	1.929(1)
Fe(1)−O(3)	2.020(3)	Fe(1)−O(6)	1.984(3)	Cu(1)−N(1)	2.077(2)
Fe(1)−O(20)	1.875(4)	Fe(1)−O(13)	1.866(5)	Cu(1)−O(3)	2.179(2)
Fe(1)−N(1)	2.198(4)	Fe(1)−N(2)	2.203(5)	Cu(1)−Cu(2)	3.4972(7)
Fe(3)−O(14)	2.042(3)	Fe(2)−O(1)	2.003(3)	Cu(2)−O(8)	1.998(2)
Fe(3)−O(16)	2.050(3)	Fe(2)−O(5)	2.028(2)	Cu(2)−O(11)	1.929(2)
Fe(3)−O(23)	2.035(3)	Fe(2)−O(3)	2.033(3)	Cu(2)−O(5)	1.913(2)
Fe(3)−O(18)	1.969(3)	Fe(2)−O(12)	2.028(3)	Cu(2)−O(6)	2.248(1)
Fe(3)−O(20)	1.876(4)	Fe(2)−O(13)	1.862(5)	Cu(2)−N(2)	2.044(2)
Fe(3)−N(4)	2.205(5)	Fe(2)−N(1)	2.213(5)		
bond angles [deg]					
$K_4[1]\cdot 25H_2O\cdot(CH_3)_2CO$		$K_3[2]\cdot 3H_2O\cdot(OH)$		$Na_3[3]\cdot 5H_2O$	
O(1)−Fe(1)−O(22)	91.9(1)	O(8)−Fe(1)−O(10)	89.8(2)	O(1)−Cu(1)−O(5)	165.38(7)
O(1)−Fe(1)−O(5)	92.0(1)	O(8)−Fe(1)−O(11)	84.6(1)	O(1)−Cu(1)−O(10)	89.11(7)
O(1)−Fe(1)−O(3)	162.8(1)	O(8)−Fe(1)−O(6)	160.8(1)	O(1)−Cu(1)−N(1)	89.88(7)
O(1)−Fe(1)−O(20)	98.3(1)	O(8)−Fe(1)−O(13)	98.3(2)	O(1)−Cu(1)−O(3)	90.46(6)
O(1)−Fe(1)−N(1)	86.9(1)	O(8)−Fe(1)−N(N2)	76.4(1)	O(5)−Cu(1)−O(10)	95.22(7)
O(22)−Fe(1)−O(5)	174.2(1)	O(10)−Fe(1)−O(11)	172.2(2)	O(5)−Cu(1)−N(1)	86.09(7)
O(22)−Fe(1)−O(3)	83.5(1)	O(10)−Fe(1)−O(6)	93.6(2)	O(5)−Cu(1)−O(3)	102.85(6)
O(22) − Fe(1) − O(20)	92.2(1)	O(10) − Fe(1) − O(13)	92.5(2)	O(10)−Cu(1)−N(1)	178.31(7)
O(22)−Fe(1)−N(1)	92.9(1)	O(10)−Fe(1)−N(2)	82.8(2)	O(10)−Cu(1)−O(3)	96.78(6)
O(5)−Fe(1)−O(3)	91.6(1)	O(11)−Fe(1)−O(6)	89.9(1)	N(1)−Cu(1)−O(3)	81.86(6)
O(5)−Fe(1)−O(20)	91.5(1)	O(11)−Fe(1)−O(13)	93.7(2)	Cu(1)−O(5)−Cu(2)	132.13(9)
O(5)−Fe(1)−N(1)	83.0(1)	O(11)−Fe(1)−N(2)	90.5(1)	O(8)−Cu(2)−O(11)	87.43(7)
O(3)−Fe(1)−O(20)	98.4(1)	O(6) − Fe(1) − O(13)	100.4(2)	O(8)−Cu(2)−O(5)	163.84(7)
O(3) − Fe(1) − N(1)	76.8(1)	O(6)−Fe(1)−N(2)	85.4(2)	O(8)−Cu(2)−O(6)	84.38(6)
O(20)−Fe(1)−N(1)	172.6(2)	O(13)−Fe(1)−N(2)	172.9(2)	O(8)−Cu(2)−N(2)	92.20(7)
O(14)−Fe(3)−O(16)	94.6(1)	O(1)−Fe(2)−O(5)	88.4(2)	O(11)−Cu(2)−O(5)	94.34(7)
O(14)−Fe(3)−O(23)	175.7(1)	O(1)−Fe(2)−O(3)	161.7(1)	O(11)−Cu(2)−O(6)	100.29(6)
O(14)−Fe(3)−O(18)	89.8(1)	O(1)−Fe(2)−O(12)	90.0(1)	O(11)−Cu(2)−N(2)	177.38(7)
O(14)−Fe(3)−O(20)	89.9(1)	O(1)−Fe(2)−O(13)	99.9(2)	O(5)−Cu(2)−O(6)	111.01(6)
O(14)−Fe(3)−N(4)	82.4(2)	O(1)−Fe(2)−N(1)	86.4(1)	O(5)−Cu(2)−N(2)	85.30(7)
O(16)−Fe(3)−O(23)	84.3(1)	O(5)−Fe(2)−O(3)	94.3(2)	O(6)−Cu(2)−N(2)	82.25(6)
O(16)−Fe(3)−O(18)	163.1(1)	O(5)−Fe(2)−O(12)	172.7(2)		
O(16)−Fe(3)−O(20)	93.7(1)	O(5)−Fe(2)−O(13)	92.7(2)		
O(16)−Fe(3)−N(4)	76.2(2)	O(5)−Fe(2)−N(1)	82.1(2)		
O(23)−Fe(3)−O(18)	90.0(1)	O(3)−Fe(2)−O(12)	85.1(1)		
O(23)−Fe(3)−O(20)	94.4(1)	O(3)−Fe(2)−O(13)	98.1(2)		
O(23)−Fe(3)−N(4)	93.3(2)	O(3)−Fe(2)−N(1)	76.1(1)		
O(18)−Fe(3)−O(20)	102.6(2)	O(12)−Fe(2)−O(13)	94.6(2)		
O(18)−Fe(3)−N(4)	88.3(2)	O(12)−Fe(2)−N(1)	90.7(1)		
O(20)−Fe(3)−N(4)	166.6(2)	O(13)−Fe(2)−N(1)	171.8(2)		

antiferromagnetic behavior was corroborated with electron paramagnetic resonance (EPR) studies. Neither the solid nor the frozen 3.0 mM aqueous solution sample of $K_4[1]\cdot 25H_2O\cdot(CH_3)_2CO$ are EPR active.

X-ray Molecular Structure Characterization. Detailed crystal structure analysis of the iron(III) complexes is described herein. The crystal structural data and selected metric data for the complexes are given in Tables 1 and 2, respectively. The thermal ellipsoid representation of the molecular structures for $K_4[1]\cdot 25H_2O\cdot(CH_3)_2CO$, $K_3[2]\cdot 3H_2O\cdot(OH)$, and $Na_3[3]\cdot 5H_2O$ are illustrated in Figures 1−3. Herein, the molecular structure of $Na_3[3]\cdot 5H_2O$ is reproduced solely for comparison reasons, otherwise its preparation and molecular structure analysis has been discussed in our previous report.[58]

Crystal Structure of $K_4[1]\cdot 25H_2O\cdot(CH_3)_2CO$. The complex crystallized in the triclinic $P\bar{1}$ space group with the unit cell comprising two tetranuclear Fe(III) complex fragments, eight potassium ions, 50 water and two acetone molecules. The thermal ellipsoid diagram of the tetranuclear Fe(III) complex anion is shown in Figure 1. The complex anion core contains four Fe(III) centers bridged by two $ccdp^{5-}$, two phthalate, and two hydroxo ligands. Each Fe(III) ion is in a distorted octahedral environment with $[NO_5]$ donor set. These structural features are similar to other tetranuclear Fe(III) complexes reported in the literature.[71,72] The Fe(1)−Fe(4) and Fe(2)−Fe(3) distances for the (μ-alkoxo) bridged binuclear subunits are 3.73(2) and 3.73(5) Å, while the Fe(1)−Fe(3) and Fe(2)−Fe(4) distances of the bis(phthalato)/(μ-hydroxo) subunits are

dx.doi.org/10.1021/ic501351a | Inorg. Chem. 2014, 53, 10974−10988

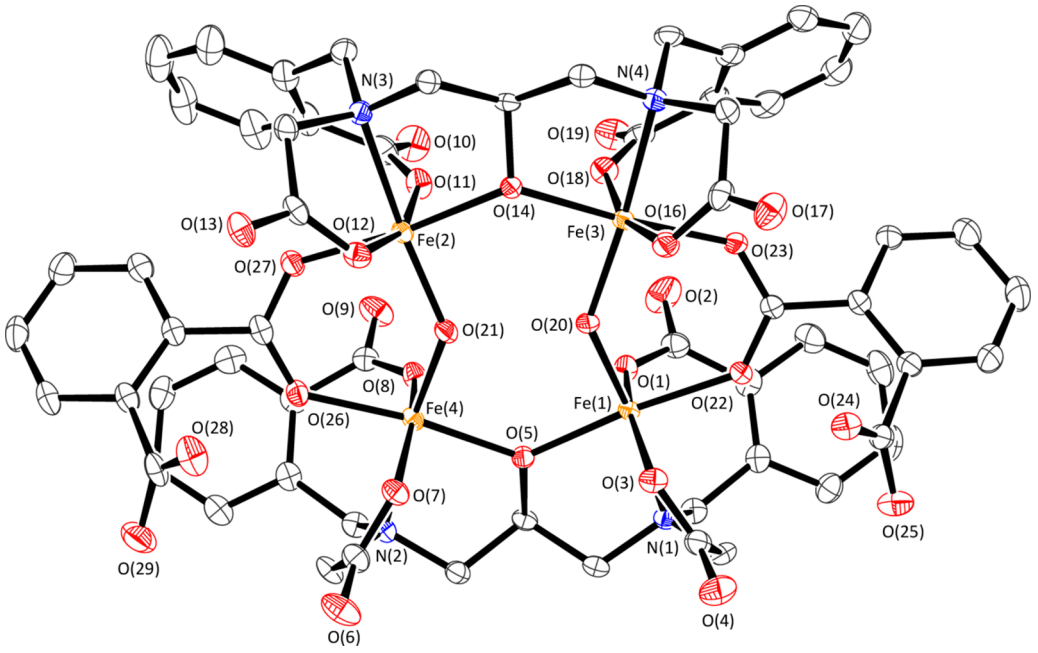

Figure 1. ORTEP drawing (50% probability) with atomic numbering scheme of the molecular structure of $K_4[\mathbf{1}]\cdot 25H_2O\cdot(CH_3)_2CO$. Hydrogen atoms, counterions, and solvent molecules of crystallization omitted for clarity.

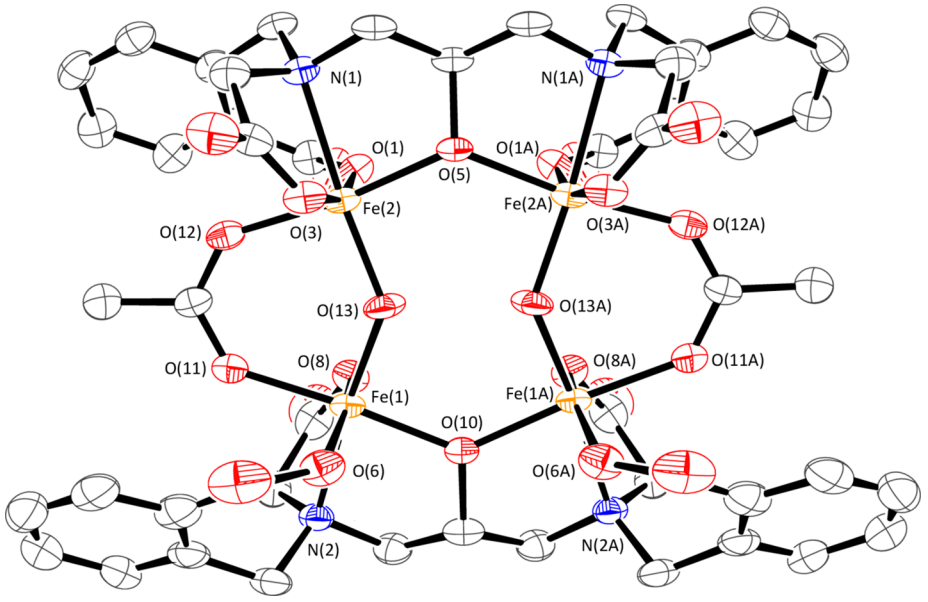

Figure 2. ORTEP drawing (50% probability) with atomic numbering scheme of the molecular structure $K_3[\mathbf{2}]\cdot 3H_2O\cdot(OH)$ including symmetry generated atoms. Hydrogen atoms, counterions, and solvent molecules of crystallization omitted for clarity.

3.46(8) and 3.36(9) Å respectively. The Fe(1)−N(1), Fe(2)−N(3), Fe(3)−N(4), and Fe(4)−N(2) bond lengths are all slightly elongated with an average distance of 2.20(7) Å. The (μ-hydroxo) bridged Fe(1)−O(20)−Fe(3) and Fe(2)−O(21)−Fe(4) bond angles of 135.2(3)° and 133.2(2)° respectively, which corresponds to similar μ-hydroxo bridged di- and tetra- nuclear Fe(III) complexes in literature.[67,72,73] The remarkable flexibility of the ccdp^{5-} ligand can be seen in the crystal structure of the complex and illustrates its ability to conform to the coordination environment and accommodate a wide variety of secondary ligands within the [Fe_4] core. This type of flexibility has also been demonstrated with several mono-, bi-, tetra-, and hexanuclear Cu(II), Co(II), Ni(II), and Zn(II) complexes of the H_5ccdp ligand.[31,51,58,74−76] The interatomic distance between O(20) and O(21) of the μ-hydroxyl groups with the [Fe_4] core at 2.41(2) Å indicates the presence of strong hydrogen bonding interaction. The [Fe_4] core of the complex is relatively planar and consists of a central puckered 8-member ring formed by four Fe(III) atoms (Fe(1), Fe(2), Fe(3), and Fe(4)), four O atoms (two μ-alkoxo (O(5) and O(14)), and two μ-hydroxo (O(20) and O(21)), Figure 4. On either side of the central ring system is a 6-member ring system consisting of the O−C−O group from the phthalato ligands as well as two Fe(III) atoms and a μ-hydroxo O atom sharing the central ring. The O(20) and O(21) of the μ-hydroxo groups are both bent slightly out of the plane and are

dx.doi.org/10.1021/ic501351a | Inorg. Chem. 2014, 53, 10974−10988

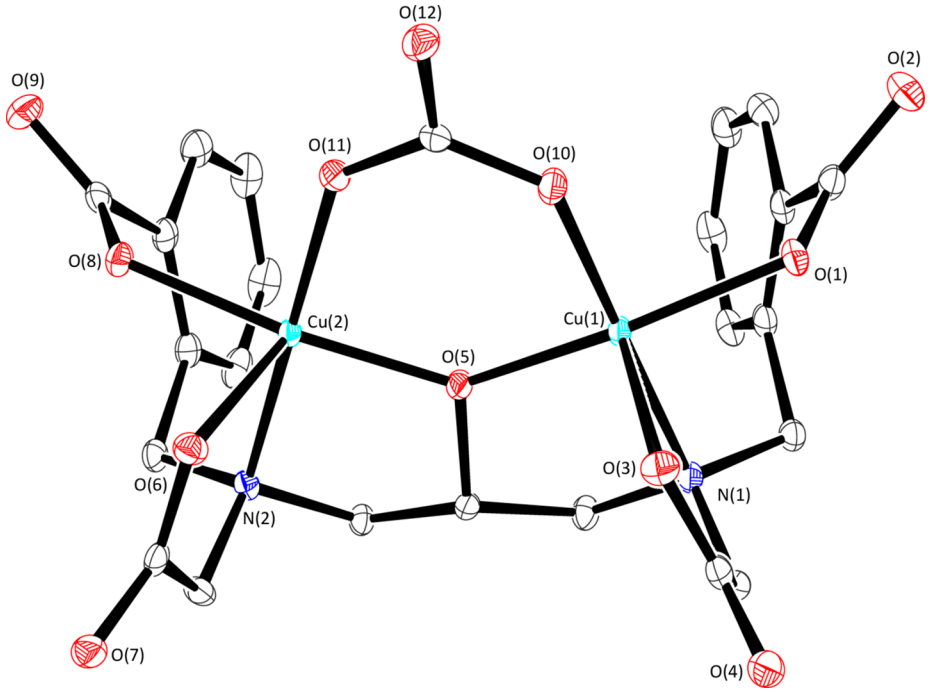

Figure 3. ORTEP drawing (50% probability) with atomic numbering scheme of the molecular structure of $Na_3[\mathbf{3}]\cdot 5H_2O$. Hydrogen atoms, counterions, and solvent molecules of crystallization omitted for clarity.

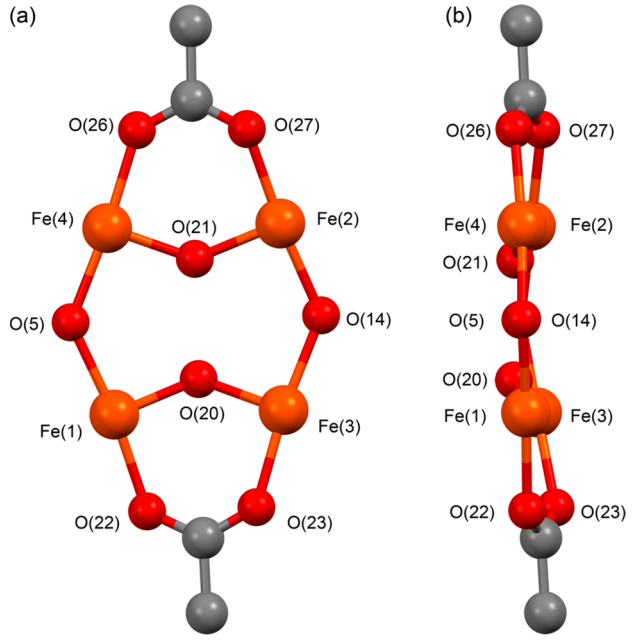

Figure 4. (a) Front view of the tetra-nuclear Fe(III) core with bridging μ-hydroxo (O20 and O21), μ-alkoxo (O5 and O14), and bridging phthalato (O22, O23 and O26, O27) groups. (b) Side view of the core of $K_4[\mathbf{1}]\cdot 2SH_2O\cdot(CH_3)_2CO$.

on opposite sides of the plane from one another. The bridging carboxylate groups of the phthalate ligands are both twisted slightly out of the plane of the core on opposite side of the plane. For both [Fe_2] units within the tetranuclear core, the $ccdp^{5-}$ ligand binds in a *cis*-fashion to the two Fe(III) ions through its aliphatic and aromatic carboxylate groups. Interestingly, the free carboxylate arms on the bridging *o*-phthalato groups are oriented in a *cis*-fashion with respect to one another and are situated in such a way that they maximize both the parallel-displaced and T-shaped intramolecular $\pi-\pi$ stacking interactions between themselves and the adjacent aromatic rings of the $ccdp^{5-}$ ligands, Figure 5.[77−80] Illustrated

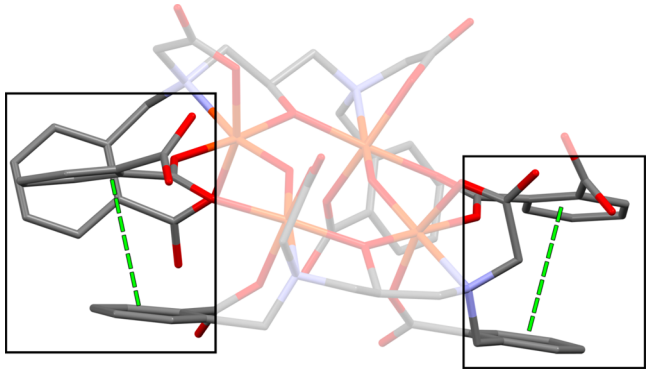

Figure 5. View of complex anion, **1**, showing the arrangement of the aromatic rings which appears to maximize both the parallel displaced and edge-on $\pi-\pi$ stacking interactions, iron (orange), nitrogen (blue), oxygen (red), and carbon (gray).

in Figure 6 are the intramolecular $\pi-\pi$ stacking interactions of the aromatic rings in an electrostatic potential map plotted from DFT calculations (B3YLP using 6-31G**) performed on the complex anion, **1**. Similarly, other views of the interactions are illustrated in the Supporting Information, Figure S5. Furthermore, the packing diagram indicates extensive hydrogen bonding which exits throughout the crystal lattice where each water of crystallization being involved in hydrogen bonding within the framework of the lattice, Supporting Information Figure S6. Potassium ions are coordinated to water molecules and free carboxylates which are not directly coordinated to the Fe(III) centers. A single potassium ion sits in the top pocket formed by the tetranuclear Fe(III) complex and stabilizes the structure through its coordination to both benzyl carboxylates

dx.doi.org/10.1021/ic501351a | *Inorg. Chem.* 2014, 53, 10974−10988

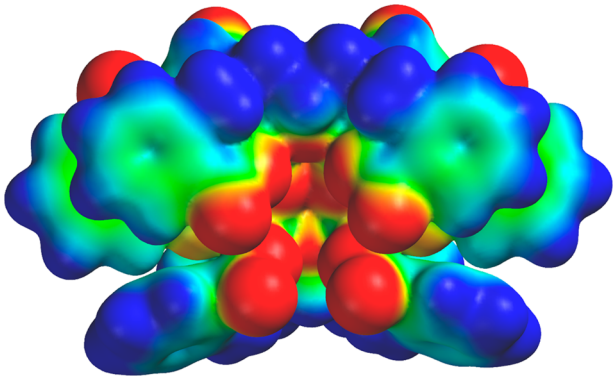

Figure 6. DFT calculations (B3YLP using 6-31G**) generated electrostatic potential map for complex anion, **1**, with Spartan (Wave function, Inc.) illustrating the intramolecular $\pi-\pi$ stacking interactions of the aromatic rings.

of each of the $ccdp^{5-}$ ligands, Supporting Information Figure S7. The extensive network of waters of hydration and potassium ions connect the two tetranuclear complex anions within the unit cell.

Crystal Structure of K_3[2]·3H_2O·(OH). The complex crystallized in the monoclinic $P2_1/m$ space group with the unit cell comprising a single tetranuclear Fe(III) complex fragment, three potassium ions, three water molecules and one hydroxide ion. The thermal ellipsoid diagram of the tetranuclear Fe(III) complex anion is shown in Figure 2. While the structural architecture of the tetranuclear Fe(III) core of K_3[**2**]·3H_2O·(OH) is very similar to that of K_4[**1**]·25H_2O·$(CH_3)_2CO$, the overall arrangement of the ligands around the core is very different. Analysis of the core structures of the two complexes, Figures 4 and 7, indicates that the core of K_3[**2**]·3H_2O·(OH) is slightly more planar than that of K_4[**1**]·25H_2O·$(CH_3)_2CO$. The bulky phthalato bridging groups of

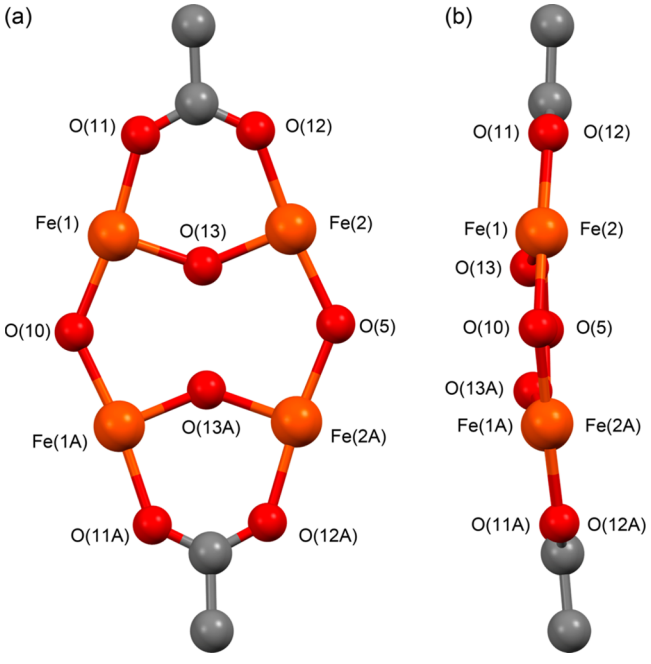

Figure 7. (a) Front view of the tetra-nuclear Fe(III) core with bridging μ-hydroxo (O13), μ-alkoxo (O5 and O10), and bridging acetate (O11 and O12) groups. (b) Side view of the core of K_3[**2**]·3H_2O·(OH).

K_4[**1**]·25H_2O·$(CH_3)_2CO$ are twisted slightly out of the plane of the ring while the smaller acetato groups are not, mainly due to factors including sterics and lack of $\pi-\pi$ stacking interactions which are present in the phthalato moiety of K_4[**1**]·25H_2O·$(CH_3)_2CO$. The replacement of the bulky bridging phthalato ligand with a much smaller bridging acetato ligand also allowed the two $ccdp^{5-}$ ligands to position themselves on opposite sides of the core in K_3[**2**]·3H_2O·(OH) while still binding in a *cis*-fashion to the two Fe(III) ions through its aliphatic and aromatic carboxylate groups as seen in K_4[**1**]·25H_2O·$(CH_3)_2CO$. This type of arrangement of the $ccdp^{5-}$ ligands may restrict the surface area of the complex anion available for solvation and may also contribute to the poor solubility of the complex in aqueous solution. The crystal structure of K_3[**2**]·3H_2O·(OH) does not show the extensive hydrogen bonding and potassium ion network that is found in K_4[**1**]·25H_2O·$(CH_3)_2CO$. Unlike to the case of K_4[**1**]·25H_2O·$(CH_3)_2CO$, and due to the absence of the phenyl ring, no $\pi-\pi$ stacking interactions were observed in K_3[**2**]·3H_2O·(OH), shown in Figure 8 and Supporting Information Figure S8. Structural data and selected metric data for the complex are presented in Tables 1 and 2, respectively.

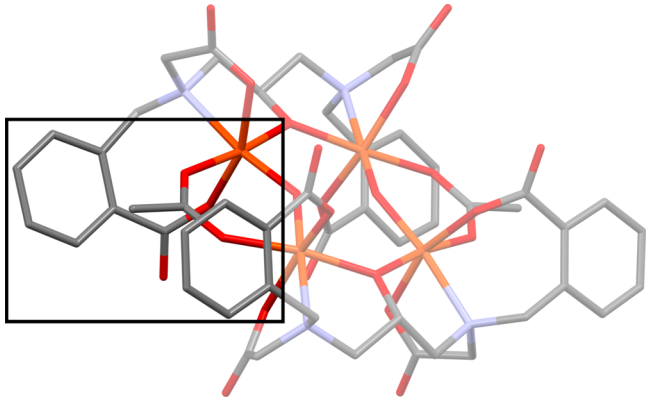

Figure 8. View of complex anion, **2**, showing the arrangement of the aromatic rings which appears to show no $\pi-\pi$ stacking interaction, iron (orange), nitrogen (blue), oxygen (red), and carbon (gray).

Carbohydrate/Metal Complex Binding Studies. Room temperature molecular interactions between D-glucose, D-mannose, D-xylose, and xylitol with K_4[**1**]·25H_2O·$(CH_3)_2CO$ and Na_3[**3**]·5H_2O were studied using UV–vis spectrometry at different pH conditions. Because of solubility differences between the two complexes, the study was carried at pH 10 and 12.5 for K_4[**1**]·25H_2O·$(CH_3)_2CO$ and Na_3[**3**]·5H_2O, respectively. The percentage distribution of the main equilibrium structures of the substrates under investigation are illustrated in Scheme 2. In an effort to obtain insights into the stability of the complexes in solution, the absorbance values for a K_4[**1**]·25H_2O·$(CH_3)_2CO$ at 477 and 600 nm and Na_3[**3**]·5H_2O at 768 nm were monitored with time for 3 h. The absorbance vs time plots (shown in Figures S9 and S10 of the Supporting Information section) clearly indicate no decay of absorption bands. Thus, stabilities of K_4[**1**]·25H_2O·$(CH_3)_2CO$ and Na_3[**3**]·5H_2O under the operative pH values were established. Several tetra-nuclear iron(III) complexes found in literature with similar structural features to K_4[**1**]·25H_2O·$(CH_3)_2CO$ and K_3[**2**]·3H_2O·(OH) presented here have been shown to be extremely stable over a wide pH range in aqueous solutions.[67,68,71,72,81,82] The K_3[**2**]·3H_2O·(OH) complex was

dx.doi.org/10.1021/ic501351a | *Inorg. Chem.* 2014, 53, 10974–10988

Scheme 2. Dominant Equilibrium Structures of D-Glucose, D-Mannose, and D-Xylose in Aqueous Solution at Room Temperature and the Structure of Xylitol

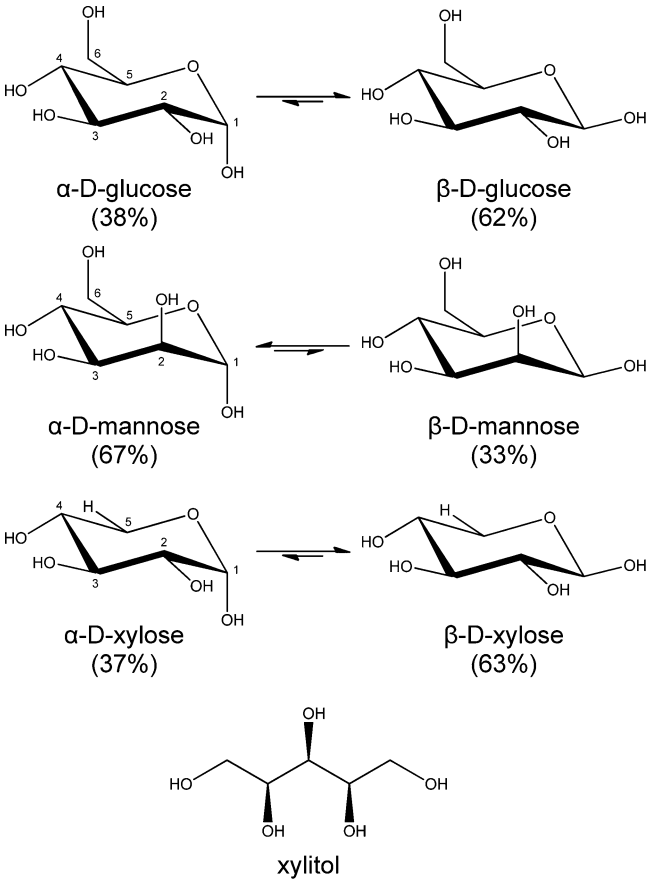

found to be insoluble in all common solvents tested and only slightly soluble in water at pH range of 4.5−5.5. Because of the very poor solubility of the complex in relevant pH ranges, no sugar binding studies using $K_3[\mathbf{2}]\cdot 3H_2O\cdot(OH)$ have been pursued.

The Rose−Drago method has been successfully employed in determination of the number of spectroscopic states, and hence the number of absorbing species, in solution in previously reported studies.[8,10,31,83] Elaborated mathematical justification of the method in relation to this study is provided in the Supporting Information section. The method as described by Connors relates to a chemical equilibrium (eq 1) in which the apparent binding constant $pK_{app} = \log(K_{app}^{-1})$, where K_{app}^{-1} is defined in eq 2.

$$[M] + [S] \leftrightarrow [MS] \quad (1)$$

$$K_{app}^{-1} = \frac{[MS]}{([M]\cdot[S])} \quad (2)$$

When considering a system in which the only absorbing species present in solution are metal complex [M] and substrate-bound metal complex [MS], a two-state system can be observed by plotting the change in absorbance at a specific wavelength of two different concentrations (j and k) versus the change in absorbance at a different wavelength of concentrations j and k; $\{(A_{1j} - A_{1k})$ versus $(A_{2j} - A_{2k})$, where $j \neq k\}$. If only one absorbing species is present in solution the graph will contain only one slope. However, in the case of a two-state system the graph will contain two different slopes passing through the origin. Furthermore, the method will also provide insight into multiple spectroscopic states exist for a given substrate−metal complex system. If a single substrate binds in multiple ways to a metal complex then multiple spectroscopic states may exist in solution depending on how many species are present. When this situation occurs it can be seen in the Rose−Drago plot by the data having nonlinear quadratic slope.[84]

The alternative route in the facile synthesis of $K_3[\mathbf{2}]\cdot 3H_2O\cdot(OH)$ by just adding CH_3CO_2K to the solution of $K_4[\mathbf{1}]\cdot 25H_2O\cdot(CH_3)_2CO$ at ambient temperature, Scheme 1, indicates that the phthalate ligand is labile, and thus can be easily displaced by an appropriate entering ligand. Similarly, the bridging carbonate ligand present in $Na_3[\mathbf{3}]\cdot 5H_2O$ can also be displaced by suitable ligands such as deprotonated carbohydrates used in this investigation. Due to the insolubility and/or instability of $K_4[\mathbf{1}]\cdot 25H_2O\cdot(CH_3)_2CO$ at pH > 11, it was necessary to carry the carbohydrate interaction study at pH 10.0 ± 0.22. Systematic additions of substoichiometric amounts of the substrates into an alkaline aqueous solutions of complex $K_4[\mathbf{1}]\cdot 25H_2O\cdot(CH_3)_2CO$ and $Na_3[\mathbf{3}]\cdot 5H_2O$ resulted in a significant reduction in the absorbance values at λ_{max} = 477, 600 nm and λ_{max} = 768 nm, respectively. The reduction in the absorption values continued with each aliquot added up to a 1:1 mol ratio of complex to substrate. Further additions of the aliquots did not bring change to the absorbance values. Similar phenomenon was observed in case of $Na_3[\mathbf{3}]\cdot 5H_2O$ as well. Shown in Figure 9 is a typical change in the λ_{max} and

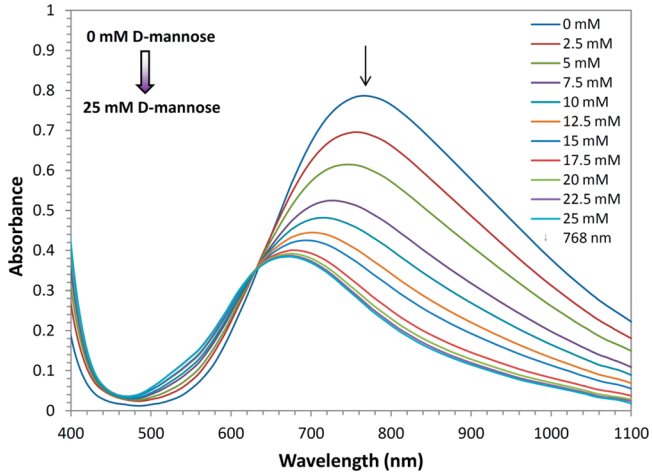

Figure 9. Selected UV−vis spectra observed during titration of $Na_3[\mathbf{3}]\cdot 5H_2O$ (5.0 mM) with D-mannose at 25 °C in unbuffered, aqueous solution at pH = 12.5; the concentration of mannose was varied from 0.0 to 25.0 mM.

absorbance values with the addition of substoichiometric amounts of the substrates into $Na_3[\mathbf{3}]\cdot 5H_2O$ solution. This particular set of data is obtained for the titration of 5.0 mM of $Na_3[\mathbf{3}]\cdot 5H_2O$ solution with aliquots of D-mannose added at 25 °C and pH of 12.5. Similar data for the rest of the systems is presented in the Supporting Information, Figure S11. While the change in the absorbance value at 768 nm for $Na_3[\mathbf{3}]\cdot 5H_2O$ was accompanied by blue shift, no such a shift was observed in the case of $K_4[\mathbf{1}]\cdot 25H_2O\cdot(CH_3)_2CO$ upon additions of the substrates. Treating such data obtained using the Rose−Drago method allowed determination of the binding stoichiometry between substrates and metal complex.[83,84]

dx.doi.org/10.1021/ic501351a | Inorg. Chem. 2014, 53, 10974−10988

The binding isotherms shown in Figure 10 represent the plot of the change in absorbance at 477 nm ($\Delta A_{477\ nm}$) versus the

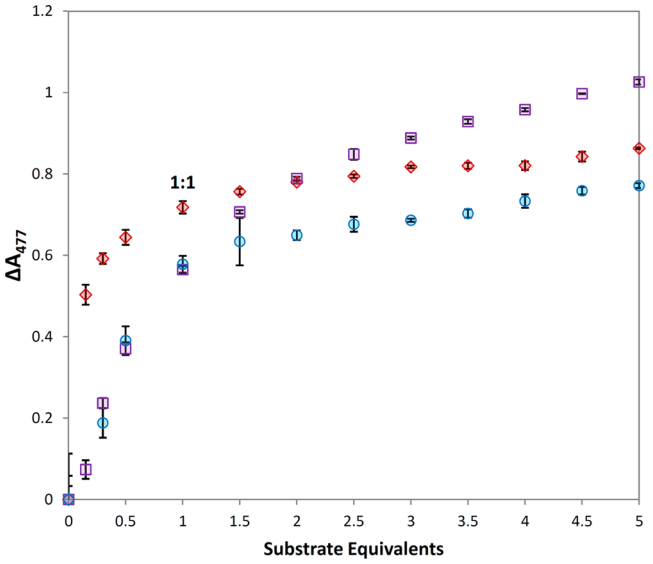

Figure 10. Binding isotherms for D-mannose, D-xylose, and xylitol. Binding isotherm plot observed during the titration of $K_4[1]\cdot 25H_2O\cdot(CH_3)_2CO$ (2.5 mM) with D-mannose (violet box), D-xylose (blue circle), and xylitol (red diamond) (0.00–12.50 mM) at 477 nm. Data collected at pH = 10.00 ± 0.22 at 25 °C.

substrate equivalents added {SE = [S]/[M_1], where [S] is the moles of the substrate and [M_1] is the moles of $K_4[\mathbf{1}]\cdot 25H_2O\cdot(CH_3)_2CO$}. The graph shows a large change in absorbance with each aliquot of substrate added up to a 1.0 equiv of substrate, followed by a plateau where additional aliquots of substrate do not significantly affect the absorbance values even up to 5.0 equiv of substrate to the $K_4[\mathbf{1}]\cdot 25H_2O\cdot(CH_3)_2CO$ solution. In the cases of D-mannose, D-xylose, and xylitol with $K_4[\mathbf{1}]\cdot 25H_2O\cdot(CH_3)_2CO$ the binding isotherms provide further spectroscopic evidence of a 1:1 binding interaction between the substrate and the complex. The data obtained for the titration of $K_4[\mathbf{1}]\cdot 25H_2O\cdot(CH_3)_2CO$ with D-glucose under the same experimental conditions was convoluted by a side reaction and thus not provided in the graph. The binding isotherm data for $Na_3[\mathbf{3}]\cdot 5H_2O$ with the applied substrates are given in the Supporting Information, Figure S12. Unlike to the case of $K_4[\mathbf{1}]\cdot 25H_2O\cdot(CH_3)_2CO$, no side reaction was observed during the titration of $Na_3[\mathbf{3}]\cdot 5H_2O$ with D-glucose, shown in Supporting Information Figure S12.

In an effort to assess the stability of the complexes toward displacement of the $ccdp^{5-}$ ligand from the complexes by any of the substrates under the experimental conditions, several control studies were carried out with aqueous solutions of the $K_4[\mathbf{1}]\cdot 25H_2O\cdot(CH_3)_2CO$ and $Na_3[\mathbf{3}]\cdot 5H_2O$ complexes as well as solutions containing a 1:3 molar ratio of the metal [M^{+n}] nitrate salts with the substrates using UV–vis spectroscopy and electrospray ionization time-of-flight mass spectrometry (ESI-MS). In a typical experiment, UV–vis spectrum of a known concentration of a complex in the presence of stoichiometric excess of a substrate in one hand and a spectrum of a free metal ion and a substrate under the same experimental conditions in the other hand were recorded and analyzed. For example, shown in Supporting Information Figure S13(a) is the UV region spectrum of an amber colored aqueous solution $K_4[\mathbf{1}]\cdot 25H_2O\cdot(CH_3)_2CO$ and xylitol in a 1:3 molar ratio, respectively. The UV region spectrum of dark orange colored solution of 2.5 mM $Fe(NO_3)_3\cdot 9H_2O$ and xylitol in a 1:3 molar ratio, respectively, in aqueous solution at pH = 10.0, 25 °C is shown in Supporting Information Figure S13(b). The visible region, d–d transition bands, of the two spectra with more concentrated concentrations are shown in Supporting Information Figure S13(c) and (d), respectively. When analyzed, the spectra from the two systems are found to be very different. The differences of the two are presented clearly both in the UV and the visible regions of the spectra. Whereas UV–vis spectrum from the $K_4[\mathbf{1}]\cdot 25H_2O\cdot(CH_3)_2CO$ and xylitol solution has absorption features at 230, 276, 477, and 600 mn, the $Fe(NO_3)_3\cdot 9H_2O$ and xylitol solution has features only at 300 and 480 nm. In a similar fashion, we studied the stability of $K_4[\mathbf{1}]\cdot 25H_2O\cdot(CH_3)_2CO$ and $Na_3[\mathbf{3}]\cdot 5H_2O$ with all the substrates and all show different UV–vis spectra, some of the results are presented in Supporting Information Figures S13–S16.

Furthermore, ESI-MS was used to investigate the stability of the complexes when interact with the substrates (Figures 11, Supporting Information S17–S19). The ESI-MS of $K_4[\mathbf{1}]\cdot 25H_2O\cdot(CH_3)_2CO$ dissolved in nanopure water with the pH adjusted to 10.0 with KOH, shown in Figure 11(a), contains signals corresponding to $[Fe_4(ccdp)_2(o\text{-phthalate})_2(OH)_2 + 7H_2O]^-$ at m/z = 1485 (13%) as well as $[Fe_4(ccdp)_2(OH)_2(H_2O)_2]^-$ at m/z = 1233 (10%), $[Fe_4(ccdp)_2(OH)_2(H_2O)_3]^{2-}$ at 625 (21%), and $[Fe_4(ccdp)_2(OH)_2]^{2-}$ at 597 (100%). The ESI-MS data shows that that the parent ion at m/z = 1486 subsequently losses *o*-phthalate and H_2O molecules to yield $[Fe_4(ccdp)_2(OH)_2(H_2O)_3]^{2-}$ and $[Fe_4(ccdp)_2(OH)_2]^{2-}$. The experimentally obtained and the simulated isotope distribution pattern for $[Fe_4(ccdp)_2(OH)_2(H_2O)_2]^-$ and $[Fe_4(ccdp)_2(o\text{-phthalate})_2(OH)_2+ 7\ H_2O]^-$ species at m/z = 1233 and 1486 are shown in Figure 11(b) and (c), respectively. The distribution patterns between the experimental and the simulated data are in excellent agreement to one another. Similarly, the ESI-MS spectra for $K_4[\mathbf{1}]\cdot 25H_2O\cdot(CH_3)_2CO$ under the same experimental conditions but in the presence of 3 mol equiv of the applied substrates was obtained (Supporting Information Figure S18). The spectra have similar features to the spectrum obtained for $K_4[\mathbf{1}]\cdot 25H_2O\cdot(CH_3)_2CO$ (Figure 11(a)) and does not contain any of the ESI-MS signals obtained from the reaction of one molar equivalent $Fe(NO_3)_3\cdot 9H_2O$ with three molar equivalents of the substrates (Supporting Information Figure S19). Similarly, the ESI-MS data collected for $Na_3[\mathbf{3}]\cdot 5H_2O$ dissolved in nanopure water with the pH adjusted to 12.5 with NaOH contains signals corresponding to $[Na_2Cu_2(ccdp)(CO_3)(H_2O)]^-$ at m/z = 721 (100%), as well $[NaHCu_2(ccdp)(CO_3)(H_2O)]^-$ at m/z = 699 (69%) and $[Cu_2(ccdp)]^-$ at m/z = 597 (58%) (Supporting Information Figure S17(a). The ESI-MS data shows that that the parent ion at m/z = 1486 subsequently losses Na^+, H^+, CO_3^{2-}, and H_2O molecules to yield $[NaHCu_2(ccdp)(CO_3)(H_2O)]^-$ and $[Cu_2(ccdp)]^-$. The experimentally obtained and the simulated isotope distribution pattern for $[Cu_2(ccdp)]^-$ and $[Na_2Cu_2(ccdp)(CO_3)(H_2O)]^-$ species at m/z = 597 and 721 are shown in Supporting Information Figure S17(b) and (c), respectively. As with $K_4[\mathbf{1}]\cdot 25H_2O\cdot(CH_3)_2CO$, the ESI-MS spectrum of $Na_3[\mathbf{3}]\cdot 5H_2O$ under the same experimental conditions but in the presence of 3 mol equiv of the substrates (Supporting Information Figure S18) was obtained as well.

dx.doi.org/10.1021/ic501351a | *Inorg. Chem.* 2014, 53, 10974–10988

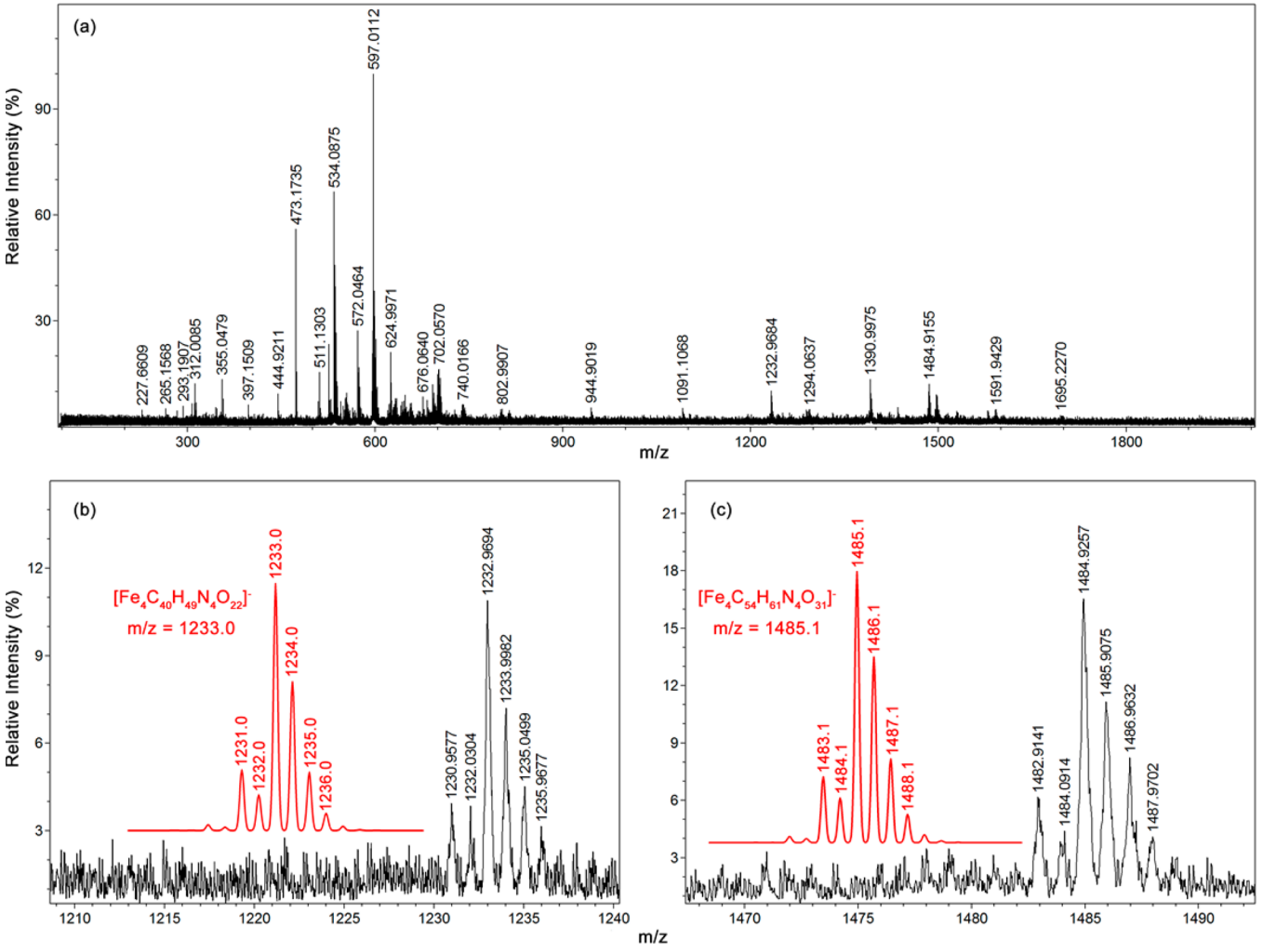

Figure 11. Negative ion mode ESI-MS spectra of a 1 mg/mL pH = 10 aqueous solution of $K_4[\mathbf{1}]\cdot 25H_2O\cdot(CH_3)_2CO$ (a) with the m/z = 1233 $[Fe_4C_{40}H_{48}N_4O_{22}]^-$ (b) and m/z = 1485 $[Fe_4C_{54}H_{62}N_4O_{31}]^-$ (c) regions expanded to show the isotope distribution patterns. Simulated isotope distribution patterns generated using Molecular Weight Calculator (Matthew Monroe, PNNL, Richland WA, U.S.A.) for the m/z = 1233 and m/z = 1485 fragments.

This spectrum also has similar features to the spectrum obtained for $Na_3[\mathbf{3}]\cdot 5H_2O$ (Supporting Information Figure S17a)) and does not contain any of the signals obtained from the reaction of one molar equivalent $Cu(NO_3)_2\cdot 3H_2O$ with three molar equivalents of the substrates (Supporting Information Figure S19).

Hence, the results of the UV−vis and the ESI-MS of the metal complexes and the control studies unambiguously establishes that the ccdp5− ligands remain firmly bound to the metal centers under the experimental conditions.

The Rose−Drago method of analysis of the UV−vis data from the titration of $K_4[\mathbf{1}]\cdot 25H_2O\cdot(CH_3)_2CO$ with D-mannose in aqueous solution at pH = 10.0 ± 0.22 produced a linear plot, Figure 12. The presence of two linear functions with different slopes which pass through the origin indicates a 1:1 binding interaction between $K_4[\mathbf{1}]\cdot 25H_2O\cdot(CH_3)_2CO$ and D-mannose as expected for two-state systems. When the data for the titration of $K_4[\mathbf{1}]\cdot 25H_2O\cdot(CH_3)_2CO$ with D-xylose (Supporting Information Figure S20) and xylitol (Supporting Information Figure S21) were subjected to the same treatment, similar results were obtained. Correspondingly, sets of similar data were obtained for the titration of $Na_3[\mathbf{3}]\cdot 5H_2O$ with the substrates as well as with D-glucose (Supporting Information Figures S22−S25). Each graph has two plots with different linear slopes which both pass through the origin, again suggesting the presence of only one substrate-bound species in solution. The core of complexes remains intact under the operative conditions of the experiment and no multiple equilibria exist in solution other than 1:1 [substrate]/[complex] ratio even with an excess of substrate.

The apparent binding constants between the complexes and the substrates were calculated and are presented in Table 3. One the basis of the value of the binding constants, the most tightly bound substrate to $K_4[\mathbf{1}]\cdot 25H_2O\cdot(CH_3)_2CO$ and to $Na_3[\mathbf{3}]\cdot 5H_2O$ is D-mannose. Subsequent to the D-mannose are the pK_{app} values for D-xylose and xylitol for $K_4[\mathbf{1}]\cdot 25H_2O\cdot(CH_3)_2CO$. When the binding constant values for $Na_3[\mathbf{3}]\cdot 5H_2O$ with D-xylose, D-mannose, and D-glucose are compared with other Cu(II) complexes values reported in the literature, they are consistently smaller. This is mainly due to the steric hindrances prompted by the molecular structure of the $ccdp^{5-}$ ligand around the Cu(II) centers. Although direct comparison of the pK_{app} values with other iron(III) complex was not possible, because of the lack of reported data, the binding constant values for $K_4[\mathbf{1}]\cdot 25H_2O\cdot(CH_3)_2CO$ are in the range of other first row transition metal complexes in literature, Table 3.

dx.doi.org/10.1021/ic501351a | Inorg. Chem. 2014, 53, 10974−10988

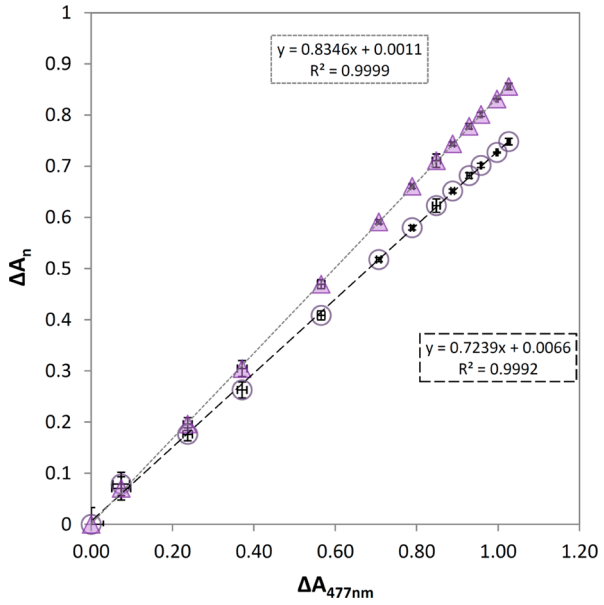

Figure 12. Plot of differences in absorbance $\Delta A_n = (A_{n,j} - A_{n,k})$ over $\Delta A_{477nm} = (A_{477nm,j} - A_{477nm,k})$ from titration of $K_4[1]\cdot 25H_2O\cdot(CH_3)_2CO$ with D-mannose where n = 490 (triangle) and 500 nm (circle) at pH = 10.00 ± 0.22, 25 °C.

In the case of Cu(II) complexes, there have been two previously reported pK_{app} values, Table 3. These two binding constant values with D-mannose as the substrate are 4.06 ± 0.03[8,9] and 2.73 ± 0.09[85] for $[Cu_2(bpdpo)]^{2+}$ and $[Cu_2(hpnbpda)(\mu\text{-OAc})]$, respectively. While the determined value of 3.43 ± 0.11 for $K_4[\mathbf{1}]\cdot 25H_2O\cdot(CH_3)_2CO$ falls within the range of these values, it binds 5-fold tighter when compared to the previously reported value (2.81 ± 0.05[32]) for the binuclear Co(II) complex, $[Co_2(tcdc)(\mu\text{-OAc})]^{2+}$. This was expected, partially due to the higher charge and greater Lewis acidity of the Fe(III) center when compared to the Cu(II) and Co(II). While previously reported pK_{app} values for $[Cu_2(bpdpo)]^{2+}$ and $[Cu_2(hpnbpda)(\mu\text{-OAc})]$ with D-xylose are 3.55 ± 0.03[8,9] and 2.51 ± 0.09,[85] respectively, Co(II) complexes with similar ligands have values of 2.93 ± 0.11[31] and 2.55 ± 0.09.[32] Hence, the 2.52 ± 0.32 value obtained for $K_4[\mathbf{1}]\cdot 25H_2O\cdot(CH_3)_2CO$ is comparable to those reported for Cu(II) and Co(II).

The only pK_{app} (2.45 ± 0.04) value for xylitol reported in the literature is with a binuclear Co(II) complex.[31] The pK_{app} values of 2.44 ± 0.12 and 2.62 ± 0.25 obtained for our complexes are comparable to that of the Co(II) complex and reflects the weakly coordinating nature of xylitol. The analysis of the binding constant values suggests that the substrate-bound complexes are reasonably stable in solution. While the interaction of simple Fe(III) ions in solution with carbohydrates and polyols has been studied and reported in literature,[42,44−46,86−88] no pK_{app} values have been determined. In general the observed the apparent binding constant values appear to be inversely related to the known pK_a values of the corresponding substrates.[6,89] It has been shown that sorbitol, D-mannose and D-glucose form complexes with M^{3+} ions under weakly basic pH conditions.[90,91] This indicates that the pK_a value is not the only factor which determines the degree of protonation of the substrates.

Although carbohydrates have multiple hydroxyl groups, which could all theoretically bind to a suitable acceptor, it has been demonstrated that binding with these types of complexes typically occur through the hydroxyl groups attached to the anomeric carbon C^1 and C^2.[8,31,32,85] The observed stronger D-mannose binding than the D-glucose or D-xylose, could be due to the difference in the configuration of the hydroxyl group at the C^2 positions. The strong binding interaction exhibited by D-mannose compared to D-xylose could have stemmed partly from structural differences between the substrates, specifically the configuration of the hydroxyl group at the C^2 position.[8,9,32,85] Specific binding modes of D-glucose have been established and previously reported in literature by using ^{13}C NMR spectroscopy technique for a dinuclear Zn(II) complex which provided strong evidence that coordination to the metal centers occurs primarily through the hydroxyl groups on C^1 and in equilibrium with the hydroxyl groups at C^2 and/or C^3.[85] Although no single crystal X-ray structure of any of the complexes is reported, similar mode of coordination with dinuclear Cu(II)[8,9,85] and Co(II)[32] complexes have been proposed in the literature. Effort continues to grow substrate bound complexes single crystals suitable for X-ray diffraction studies. The $K_4[\mathbf{1}]\cdot 25H_2O\cdot(CH_3)_2CO$ complex is sterically more congested than $Na_3[\mathbf{3}]\cdot 5H_2O$ and therefore it is unlikely that the C^3 hydroxyl of D-mannose would participate in binding in the former. The proposed binding of the substrates to the complexes through the hydroxyl groups of C^1 and C^2 is shown in Scheme 3.

EXPERIMENTAL SECTION

General Remarks. All starting materials were purchased from commercial sources and were used without further purification. Elemental analyses were determined by Atlantic Microlab, Norcross, GA. FT-IR spectra were recorded on solid samples using a Bruker Vector 22 FTIR-ATR spectrometer. Room temperature magnetic studies on the complexes were carried out on a Johnson Matthey MSB Mk1 magnetic susceptibility balance with standard (4 mm OD × 3.24 mm ID) sample tubes and using $CuSO_4\cdot 5H_2O$ as a callibrant. DFT calculations on $K_4[\mathbf{1}]\cdot 25H_2O\cdot(CH_3)_2CO$ were carried out using the Spartan '10 software suite from Wavefunction, Inc.,[92] with the B3LYP functional[93,94] and 6-31-G** basis set in vacuum. Experimental X-ray crystal structure data was imported and used for the calculations with

Table 3. Apparent Binding Constants ($pK_{app} = \log(K_{app}^{-1})$) for the Substrate Bound to the Complexes

complex	D-mannose	D-glucose	D-xylose	xylitol	ref
1, $[Fe_4(ccdp)_2(o\text{-phth})_2(OH)_2]^{4-}$	3.43 ± 0.11		2.52 ± 0.32	2.44 ± 0.12	this work[a]
3, $[Cu_2(ccdp)(\mu\text{-}CO_3)]^{3-}$	2.62 ± 0.25	1.94 ± 0.43	2.25 ± 0.11	2.43 ± 0.08	this work[b]
$[Cu_2(bpdpo)]$	4.06 ± 0.03	2.56 ± 0.03	3.55 ± 0.03		8, 9
$[Cu_2(hpnbpda)(\mu\text{-OAc})]$	2.73 ± 0.09	2.46 ± 0.08	2.51 ± 0.04		85
$[Co_2(ccdp)(\mu\text{-}CO_3)]$		2.59 ± 0.19	2.93 ± 0.11	2.45 ± 0.04	31
$[Co_2(tcdc)(\mu\text{-OAc})]$	2.81 ± 0.05	2.48 ± 0.15	2.55 ± 0.09		32

[a] $K_4[\mathbf{1}]\cdot 25H_2O\cdot(CH_3)_2CO$ at pH = 10.0 ± 0.22. [b] $Na_3[\mathbf{3}]\cdot 5H_2O$ at pH = 12.5 ± 0.21.

dx.doi.org/10.1021/ic501351a | Inorg. Chem. 2014, 53, 10974−10988

Scheme 3. Proposed Carbohydrate Binding Modes to the Complex Ions of 1 and 3

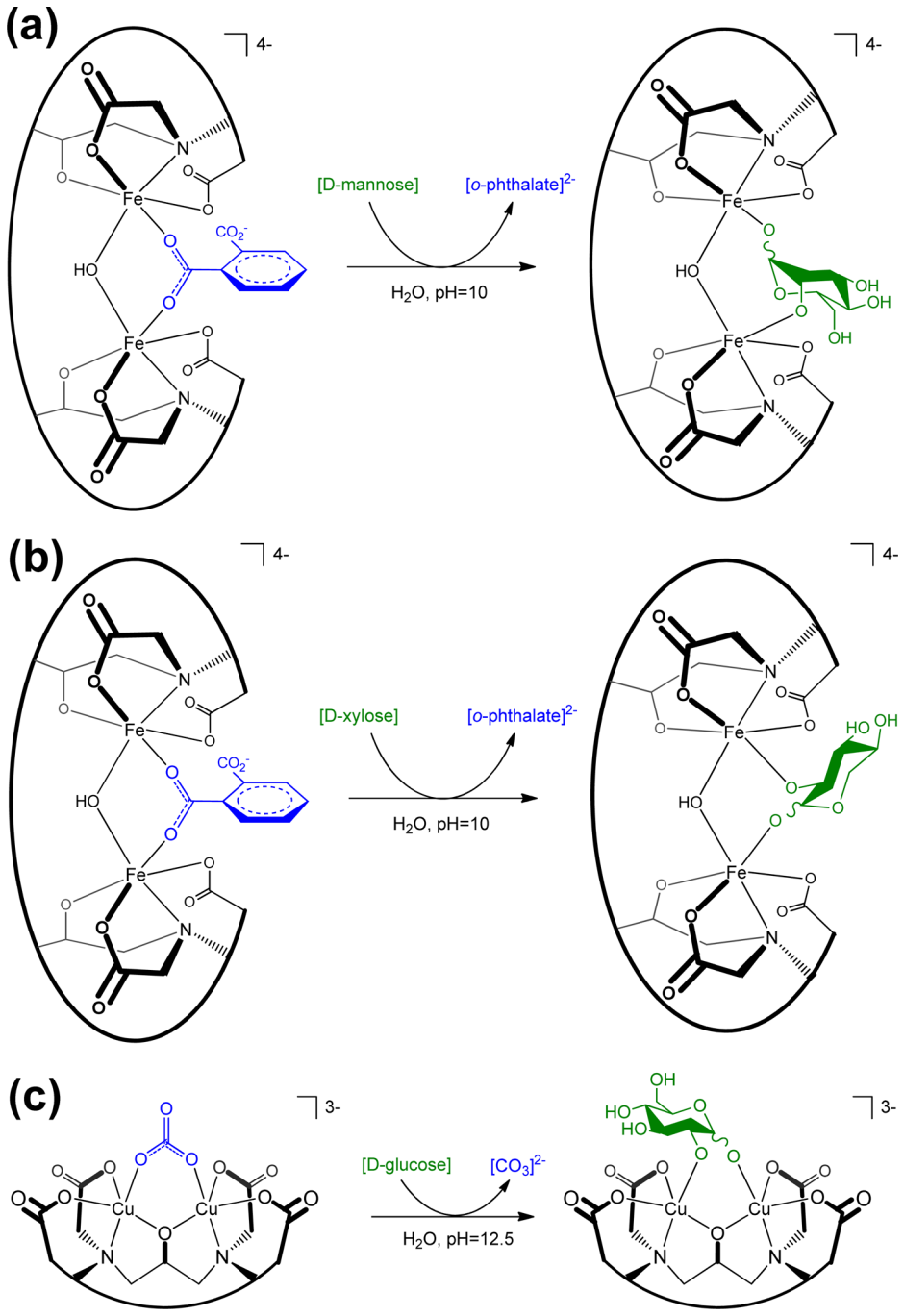

heavy atoms frozen to determine the energy as well as generate the electrostatic potential map. Furthermore, the number of unpaired electrons in the complex as calculated from the room temperature magnetic study was incorporated into the calculation to more accurately account for the antiferromagnetic coupling between the Fe(III) centers.

UV–vis Spectroscopy. All experiments were performed on an Agilent 8453 diode array UV–vis spectrophotometer with 1 cm quartz cell at room temperature over a range of 200–900 nm. An Eppendorf Research micropipette was used to measure volumes. All experiments were carried out in degassed nanopure water, in which pH of the solutions adjusted using either NaOH or KOH solution. Typically, 10.0 mmol stock solution of complex **1** and 50.0 mmol stock solutions of each carbohydrates were prepared separately and kept at room temperature. The total concentration of $K_4[\mathbf{1}]\cdot 25H_2O\cdot(CH_3)_2CO$ ($V_{\text{complex }\mathbf{1}}$ = 1 mL; $[\text{Complex}]_t$ = 2.5 mmol) and the total volume of the resulting solutions (V_t = 4 mL) were kept constant during the titration experiments ($V_{\text{substrate}}$ = 0–1000 μL) by adding an appropriate amount of water in which the pH had been adjusted to 10.0. For $Na_3[\mathbf{3}]\cdot 5H_2O$, to a $[\text{Complex}]_t$ = 2.5 mmol of V_t = 25 mL a total of 0.625 mmol in an increments of 0.0625 mmol of solid carbohydrate samples were added at pH ~12.5. The UV–vis absorbance and the pH meter readings of the resulting mixtures were measured within 15 min after mixing. Each concentration was made and measured three times and the data points were averaged. Standard deviation was applied to these averages.

Mass Spectrometry. Electrospray ionization time-of-flight mass-spectrometry (ESI-TOF-MS) spectrometry data was collected using a Bruker Daltonics micrOTOF instrument. Data was collected for a m/z range of 100–2000 in both positive and negative ion modes. Samples

dx.doi.org/10.1021/ic501351a | Inorg. Chem. 2014, 53, 10974–10988

were delivered as dilute (1−2 mg/mL) aqueous and methanol solutions with a relatively moderate flow rate of 1.00 mL/h. In all the measurements, the setting of the nebulization gas, N_2, was 45.0 psi, the capillary potential was 4 kV, the drying gas was 5.0 L/min, the skimmer was set to −60 V, and the hexapole RF was set to 400 Vpp. Simulations of the stable isotope patterns were made using Molecular Weight Calculator (Matthew Monroe, PNNL, Richland WA, U.S.A.) software.

Synthesis of *N,N′*-Bis[2-carboxybenzomethyl]-*N,N′*-Bis-[carboxymethyl]-1,3-diaminopropan-2-ol, H_5ccdp. The ligand has been prepared according to our previously published procedure.[51] The product was collected by filtration, washed with water, methanol and dried at 80 °C. The product was confirmed by elemental analysis, FTIR and ^{1}H and ^{13}C NMR spectroscopy. Yield: 5.2 g (95%). Anal. Calcd for $C_{23}H_{26}N_2O_9{\cdot}2HCl$: C, 50.47%; H, 5.16%; N, 5.12%. Found: C, 50.31%; H, 5.50%; N, 5.06%. FTIR (cm-1): ν = 3503(b), 3032(b), 1667(s), 1590(vs), 1562(s), 1440(s), 1392(s), 1264(s), 1160(s), 902(s), 845(s), 788(s). ^{1}H NMR for the sodium salt of the compound (500 MHz, D_2O, 25 °C, δ): 7.51 (d, 2H, J = 7.5 Hz), 7.40 (m, 4H), 7.33 (t, 2H, J = 7.5 Hz), 3.92 (d, 2H, J = 13.5 Hz), 3.82 (d, 2H, J = 13.5 Hz), 3.71 (quin, 1H), 3.19 (d, 2H, J = 16.5 Hz), 3.10 (d, 2H, J = 16.5 Hz), 2.62 (d, 1H, J = 3.0 Hz), 2.59 (d, 1H, J = 3.0 Hz), 2.45 (d, 1H, J = 9.0 Hz), 2.42 (d, 1H, J = 9.0). ^{13}C NMR (500 MHz, D_2O, 25 °C, δ): 180.14, 178.80, 140.58, 134.41, 130.46, 128.48, 127.30, 126.42, 66.27, 58.70, 58.57, 56.68.

Synthesis of $K_4[Fe_4(ccdp)_2(o\text{-phth})_2(OH)_2]{\cdot}25H_2O{\cdot}(CH_3)_2CO$ (K_4[1]$\cdot25H_2O\cdot(CH_3)_2CO$). A methanol−$H_2O$ solvent mixture (3:1 by vol.) (5.5 mL) containing $FeCl_3{\cdot}6H_2O$ (0.9942 g, 3.68 mmol) was added dropwise, at ambient temperature, to a stirring 10 mL methanol−H_2O solution (3:1 by vol.) of the ligand H_5ccdp (1.0034 g, 1.83 mmol), phthalic acid (0.3046 g, 1.83 mmol), and $KHCO_3$ (1.4682 g, 14.67 mmol). After complete addition the resulting green solution was refluxed for 30 min and then allowed to cool to ambient temperature for 2 h. The green precipitate that formed was gravity filtered, washed with one 10 mL portion of H_2O, and dried overnight at 70 °C. X-ray quality single crystals of K_4[**1**]$\cdot25H_2O\cdot(CH_3)_2CO$ were grown by acetone diffusion into an aqueous solution of the complex. Yield: 1.6643 g (44%). Anal. Calcd for $C_{65}H_{108}Fe_4K_4N_4O_{54}$: C, 35.66; H, 4.97; N, 2.56. Found: C, 35.67; H, 4.93; N, 2.55%. ESI-MS m/z (%): 597.0112 (100) $[Fe_4C_{46}H_{44}N_4O_{20}]^{2-}$; 624.9971 (21) $[Fe_4C_{46}H_{50}N_4O_{23}]^{2-}$; 1233 (10) $[Fe_4C_{46}H_{49}N_4O_{22}]^{-}$; 1484.9155 (13) $[Fe_4C_{54}H_{61}N_4O_{31}]^{-}$. IR (Solid on ATR): ν 3391 (br) 1716 (w) 1613, 1596, 1571, 1538 (s) 1365 (s) 1152 (m), 1076, 1040, 991, 963, 928, 872, 829 (m), 758, 710, 663 (s) (cm^{-1}). UV−vis (H_2O) λ_{max}/nm (ε/L mol^{-1} cm^{-1}): 600 (119), 477 (528)^{sh}, 276 (19404)^{sh}, 230 (34675)^{sh}. μ_{eff} (296 K): 4.93.

Synthesis of $K_3[Fe_4(ccdp)_2(OAc)_2(OH)_2](OH){\cdot}3H_2O$ (K_3[2]$\cdot3H_2O\cdot$(OH)) . A methanol−H_2O solvent mixture (3:1 by vol) (5.5 mL) containing $FeCl_3{\cdot}6H_2O$ (1.0143 g, 3.75 mmol) was added dropwise, at ambient temperature, to a stirring 10 mL methanol−H_2O solution (3:1 by vol) of the ligand H_5ccdp (1.0228 g, 1.87 mmol), CH_3CO_2K (0.1834 g, 1.87 mmol), and $KHCO_3$ (1.1241 g, 11.23 mmol). After complete addition, the resulting yellow-green solution was refluxed for 30 min and then allowed to cool to ambient temperature for 2 h. The yellow-green precipitate that formed was gravity filtered, washed with one 10 mL portion of H_2O, and dried overnight at 70 °C. X-ray quality single crystals of K_3[**2**]$\cdot3H_2O\cdot$(OH) were grown by slow acetone diffusion into a very dilute aqueous solution of the complex. Yield: 1.5417 g (55%). Similarly, an aqueous solution of K_4[**1**]$\cdot25H_2O\cdot(CH_3)_2CO$ was treated with an excess of CH_3CO_2K and left to stirring for 16 h at room temperature to produce K_3[**2**]$\cdot3H_2O\cdot$(OH) in even higher yields. Anal. Calcd for $C_{50}H_{63}Cl_9Fe4K_{12}N_4O_{31}$: C, 26.96; H, 2.85; N, 2.51. Found: C, 26.57; H, 2.83; N, 2.51%. IR (Solid on ATR): ν 3396 (br) 1609, 1599, 1572, 1541 (s) 1487, 1439 (w) 1365 (s) 1150 (m), 1071, 1035, 990, 965 (w) 925 (w, sh) 909, 872 (m), 761, 714, 661 (s) (cm^{-1}). UV−vis (H_2O) λ_{max}/nm (ε/L mol^{-1} cm^{-1}): 477 (456), 355 (4823)^{sh}, 275 (15122)^{sh}, 228 (30672)^{sh}.

Synthesis of $Na_3[Cu_2(ccdp)(\mu\text{-}CO_3)]{\cdot}5H_2O$ (Na_3[3]$\cdot5H_2O$). The complex has been prepared in a similar manner to our previously published procedure.[51] A methanoic solution (5 mL) of $Cu(ClO_4)_2{\cdot}6H_2O$ (0.313 g, 0.845 mmol) was added dropwise, at ambient temperature with stirring, to a 16 mL methanoic solution of the ligand H_5ccdp (0.200 g, 0.422 mmol) and NaOH (0.1014 g, 2.54 mmol), which was first dissolved in water (1 mL) and then added to the ligand-methanol mixture over a period of 15 min. After complete addition, a layer of blue was seen separating in solution. The whole reaction was stirred overnight at room temperature. The solution was filtered using gravity filtration and the filtrate was setup for crystallization. The X-ray quality single crystals were grown by slow acetone-H_2O (6:1 by vol) diffusion into the methanoic solution of the complex. Yield: 0.1633 g (47%). Anal. Calcd for $C_{24}H_{55}Cu_2N_2Na_3O_{29}$: C, 27.94; H, 5.37; N, 2.72. Found: C, 28.02; H, 5.19; N, 2.73%. ESI-MS m/z (%): 597.0146 (58) $[Cu_2C_{23}H_{21}N_2O_9]^{-}$; 699.0683 (69) $[NaCu_2C_{24}H_{23}N_2O_{13}]^{-}$; 721.0455 (100) $[Na_2Cu_2C_{24}H_{23}N_2O_{13}]^{-}$. UV−vis ($H_2O$) λ_{max}/nm (ε/L mol^{-1} cm^{-1}): 768 (143), 270 (5744)^{sh}.

X-ray Crystallography and Data Analysis. The data were collected at 98(2) K using a Rigaku AFC12/Saturn 724 CCD fitted with Mo Kα radiation (k = 0.71073 Å). Data collection and unit cell refinement were performed using CRYSTAL CLEAR software.[95] The total number of data was measured in the range 3.09° < θ < 27.5° using ω scans. Data processing and absorption correction, giving minimum and maximum transmission factors, were accomplished with CRYSTAL CLEAR and ABSCOR, respectively.[96] The structure, using SHELXL-97, was solved by direct methods and refined (on F^2) using full-matrix, least-squares techniques.[97,98] All non-hydrogen atoms, for all structures, were refined with anisotropic displacement parameters. All carbon bound hydrogen atom positions were determined by geometry and refined by a riding model. Electron density peaks were used to identify oxygen bound hydrogen atoms and the displacement parameters were set to 1.5 times the displacement parameters of the bonded atoms. Electron density peaks were used to identify the carbon bound hydrogen atoms for the carbon labeled C14, in the molecular structure of K_4[**1**]$\cdot25H_2O\cdot(CH_3)_2CO$, and the displacement parameters were set to 1.2 times the displacement parameters of the carbon atom.

CONCLUSIONS

Selective affinity and specific modes of substrate binding are vital in biological functions, be it for recognition, catalysis, signaling or numerous other cell operations. Inspired by such systems, we synthesized and investigated new tetra-iron(III) and di-copper(II) complexes, K_4[**1**]$\cdot25H_2O\cdot(CH_3)_2CO$, K_3[**2**]$\cdot3H_2O\cdot$(OH), and Na_3[**3**]$\cdot5H_2O$, for potential interaction with biologically important carbohydrates in aqueous alkaline solution. Whereas K_4[**1**]$\cdot25H_2O\cdot(CH_3)_2CO$ and Na_3[**3**]$\cdot5H_2O$ are very soluble and stable in solutions at pH 10.0 and 12.5, respectively, K_3[**2**]$\cdot3H_2O\cdot$(OH) is slightly soluble only at pH ranges (4−5) that are not suitable for the substrate binding studies. Our investigation into the interactions of D-mannose, D-glucose, D-xylose, and xylitol with either K_4[**1**]$\cdot25H_2O\cdot(CH_3)_2CO$ or Na_3[**3**]$\cdot5H_2O$ reveals that only 1:1 substrate/complex molar ratio are formed and sustained in solution, even in the presence of stoichiometric excess of the substrate. Based on the determined binding constant values, pK_{app}, the most tightly bound substrate to K_4[**1**]$\cdot25H_2O\cdot(CH_3)_2CO$ and to Na_3[**3**]$\cdot5H_2O$ is D-mannose. The coordination D-mannose to the Fe(III) complex is favored over the Cu(II) complex by an order of magnitude. However, the molecularly small substrates, D-xylose and xylitol, displays somewhat similar coordination affinity toward K_4[**1**]$\cdot25H_2O\cdot(CH_3)_2CO$ and Na_3[**3**]$\cdot5H_2O$. While the nature of D-glucose binding to the Cu(II) complex is similar to the other substrates used in this study, D-glucose interaction with the Fe(III) complex, however, is complicated by an associated side reaction that we are currently investigating. Direct structural evidence, from single crystal X-

dx.doi.org/10.1021/ic501351a | Inorg. Chem. 2014, 53, 10974−10988

ray structure, for these complexes is presently unavailable. However, our previously reported NMR study on the Zn(II) analog of the complex suggested that binding of the carbohydrates with these types of complexes occur through the hydroxyl groups attached to the anomeric carbon, C^1, and C^2. The current investigation on the interaction and pK_{app} value determination between the complexes and the sugars positively contributes to the field of carbohydrate recognition in aqueous media. Additionally, the present study provides important structural and functional information relevant to various sugar-metabolizing metalloenzymes and catalysis.

■ ASSOCIATED CONTENT

Supporting Information

The X-ray crystallographic data in CIF format for complexes $K_4[\mathbf{1}]\cdot 25H_2O\cdot(CH_3)_2CO$ and $K_3[\mathbf{2}]\cdot 3H_2O\cdot(OH)$, UV−vis, IR data, ESI-MS data, figures of the substrate/complex interactions, binding isotherms, partial views of molecular structures of $K_4[\mathbf{1}]\cdot 25H_2O\cdot(CH_3)_2CO$ and $K_3[\mathbf{2}]\cdot 3H_2O\cdot(OH)$, and Rose−Drago graphs. This material is available free of charge via the Internet at http://pubs.acs.org.

■ AUTHOR INFORMATION

Corresponding Author

*Fax (210)458-7428. E-mail: ghezai.musie@utsa.edu.

Notes

The authors declare no competing financial interest.

■ ACKNOWLEDGMENTS

Financial support from the Welch Foundation in the form of Grant AX-1540 and the Department of Chemistry at UTSA are greatly appreciated. The authors also would like to thank the Chemistry Department, University of Texas at San Antonio, for funds to upgrade the X-ray instrument and computers. Special thanks to Dr. David Black for helping with the ESI-MS measurements and valuable discussions on the data.

■ REFERENCES

(1) Lis, H.; Sharon, N. *Chem. Rev.* **1998**, *98*, 637−674.
(2) Sears, P.; Wong, C.-H. *Angew. Chem., Int. Ed.* **1999**, *38*, 2300−2324.
(3) Chen, E. H.; Hayes, P. L.; Nguyen, S. T.; Geiger, F. M. *J. Phys. Chem. C* **2010**, *114*, 19483−19488.
(4) Garcia, L.; Maisonneuve, S. P.; Xie, J.; Guillot, R. G.; Dorlet, P.; Rivière, E.; Desmadril, M.; Lambert, F. O.; Policar, C. *Inorg. Chem.* **2010**, *49*, 7282−7288.
(5) Klüfers, P.; Kunte, T. *Angew. Chem., Int. Ed.* **2001**, *40*, 4210−4212.
(6) Norkus, E.; Vaičiūnien, J.; Vuorinen, T.; Gaidamauskas, E.; Reklaitis, J.; Jääskeläinen, A.-S.; Crans, D. C. *Carbohydr. Res.* **2004**, *339*, 599−605.
(7) Pidko, E. A.; Degirmenci, V.; Van Santen, R. A.; Hensen, E. J. M. *Inorg. Chem.* **2010**, *49*, 10081−10091.
(8) Striegler, S.; Dittel, M. *J. Am. Chem. Soc.* **2003**, *125*, 11518−11524.
(9) Striegler, S.; Dittel, M. *Inorg. Chem.* **2005**, *44*, 2728−2733.
(10) Striegler, S.; Tewes, E. *Eur. J. Inorg. Chem.* **2002**, *2002*, 487−495.
(11) Davis, A. P.; Wareham, R. S. *Angew. Chem., Int. Ed.* **1999**, *38*, 2978−2996.
(12) Pullman, B.; Goldblum, N. *Metal−Ligand Interactions in Organic Chemistry and Biochemistry*; D. Reidel Pub. Co.: Dordrecht, the Netherlands, 1977.
(13) Wong, C.-H. *Acc. Chem. Res.* **1999**, *32*, 376−385.
(14) Gyurcsik, B.; Nagy, L. *Coord. Chem. Rev.* **2000**, *203*, 81−149.
(15) Piarulli, U.; Floriani, C. *Assembling Sugars and Metals: Novel Architectures and Reactivities in Transition Metal Chemistry*, Progress in Inorganic Chemistry, Volume *45*; John Wiley & Sons, Inc.: Hoboken, NJ, 2007; pp 393−429.
(16) Whitfield, D. M.; Stojkovski, S.; Sarkar, B. *Coord. Chem. Rev.* **1993**, *122*, 171−225.
(17) Borriello, C.; Cucciolito, M. E.; Panunzi, A.; Ruffo, F. *Inorg. Chim. Acta* **2003**, *353*, 238−244.
(18) Hashizume, T.; Yonehara, K.; Ohe, K.; Uemura, S. *J. Org. Chem.* **2000**, *65*, 5197−5201.
(19) Hu, X.; Zhang, W.; Carmichael, I.; Serianni, A. S. *J. Am. Chem. Soc.* **2010**, *132*, 4641−4652.
(20) Mazik, M.; Cavga, H.; Jones, P. G. *J. Am. Chem. Soc.* **2005**, *127*, 9045−9052.
(21) Ouchi, K.; Saito, S.; Shibukawa, M. *Inorg. Chem.* **2013**, *52*, 6239−6241.
(22) Saha, B.; Rajanbabu, T. V. *Org. Lett.* **2006**, *8*, 4657−4659.
(23) Terraneo, G.; Potenza, D.; Canales, A.; Jiménez-Barbero, J.; Baldridge, K. K.; Bernardi, A. *J. Am. Chem. Soc.* **2007**, *129*, 2890−2900.
(24) Yang, L.; Hua, X.; Xue, J.; Pan, Q.; Yu, L.; Li, W.; Xu, Y.; Zhao, G.; Liu, L.; Liu, K.; Chen, J. E.; Wu, J. *Inorg. Chem.* **2011**, *51*, 499−510.
(25) Feig, A. L.; Lippard, S. J. *Chem. Rev.* **1994**, *94*, 759−805.
(26) Kato, M.; Tanase, T.; Mikuriya, M. *Inorg. Chem.* **2006**, *45*, 2925−2941.
(27) Lippard, S. J. B., Jeremy, M. *Principles of Bioinorganic Chemistry*; University Science Books: Mill Valley, CA, 1994; p 411.
(28) Tshuva, E. Y.; Lippard, S. J. *Chem. Rev.* **2004**, *104*, 987−1012.
(29) Kumaran, D.; Bonanno, J. B.; Burley, S. K.; Swaminathan, S. *Proteins: Struct., Funct., Bioinf.* **2006**, *64*, 851−862.
(30) Gultneh, Y.; Farooq, A.; Liu, S.; Karlin, K. D.; Zubieta, J. *Inorg. Chem.* **1992**, *31*, 3607−3611.
(31) Bera, M.; Curtiss, A. B. S.; Musie, G. T.; Powell, D. R. *Inorg. Chem.* **2012**, *51*, 12093−12101.
(32) Bera, M.; Patra, A. *Carbohydr. Res.* **2011**, *346*, 733−738.
(33) Burger, J.; Klüfers, P. *Z. Anorg. Allg. Chem.* **1998**, *624*, 359−360.
(34) Larrabee, J. A.; Chyun, S.-A.; Volwiler, A. S. *Inorg. Chem.* **2008**, *47*, 10499−10508.
(35) Xeng, Y. H.; Han, J.; Zhou, G. H.; Sun, Z.; Zhang, X. J.; Zhang, B. L.; Zhang, Y. H.; Yuan, H. Q.; Ge, M. F. *J. Coord. Chem.* **2008**, *61*, 715−730.
(36) Adams, H.; Bradshaw, D.; Fenton, D. E. *Dalton Trans.* **2001**, *2001*, 3407−3409.
(37) Adams, H.; Bradshaw, D.; Fenton, D. E. *Dalton Trans.* **2002**, *2002*, 925−930.
(38) Bandwar, R. P.; Rao, C. P. *Curr. Sci.* **1997**, *72* (11), 788.
(39) Barker, R.; Serianni, A. S. *Acc. Chem. Res.* **1986**, *19*, 307−313.
(40) E. Alekseev, Y.; D. Garnovskii, A.; A. Zhdanov, Y. *Russ. Chem. Rev.* **1998**, *67*, 649−669.
(41) Kaiwar, S. P.; Raghavan, M. S. S.; Rao, C. P. *Dalton Trans.* **1995**, *1995*, 1569−1576.
(42) Ferrari, E.; Saladini, M. *J. Inorg. Biochem.* **2004**, *98*, 1002−1008.
(43) Spiro, T. G.; Saltman, P. *Polynuclear Complexes of Iron and Their Biological Implications*, Structure and Bonding; Jørgensen, C. K., Neilands, J. B., Nyholm, R., Reinen, D., Williams, R. J. P., Eds.; Springer: Berlin, 1969; Vol. *6*, pp 116−156.
(44) Charley, P. J.; Sarkar, B.; Stitt, C. F.; Saltman, P. *Biochim. Biophys. Acta* **1963**, *69*, 313−321.
(45) Davis, P. S.; Deller, D. J. *Nature* **1966**, *212*, 404−405.
(46) Rao, C. P.; Geetha, K.; Raghavan, M. S. S.; Sreedhara, A.; Tokunaga, K.; Yamaguchi, T.; Jadhav, V.; Ganesh, K. N.; Krishnamoorthy, T.; V.A. Ramaiah, K.; Bhattacharyya, R. K. *Inorg. Chim. Acta* **2000**, *297*, 373−382.
(47) Saltman, P. *J. Chem. Educ.* **1965**, *42*, 682.
(48) Bandwar, R. P.; Rao, C. P. *J. Inorg. Biochem.* **1997**, *68*, 1−6.
(49) Krishnamoorthy, T.; Sreedhara, A.; Rao, C. P.; Ramaiah, K. V. A. *Arch. Biochem. Biophys.* **1998**, *349*, 122−128.
(50) Bandwar, R. P.; Giralt, M.; Hidalgo, J.; Rao, C. P. *Carbohydr. Res.* **1996**, *284*, 73−84.

(51) Curtiss, A. B. S.; Bera, M.; Musie, G. T.; Powell, D. R. *Dalton Trans.* **2008**, *2008*, 2717−2724.
(52) Bera, M.; Musie, G. T.; Powell, D. R. *Inorg. Chem. Commun.* **2008**, *11*, 293−299.
(53) Bera, M.; Musie, G. T.; Powell, D. R. *Inorg. Chem.* **2009**, *48*, 4625−4627.
(54) Bera, M.; Wong, W. T.; Aromí, G.; Ray, D. *Eur. J. Inorg. Chem.* **2005**, *2005*, 2526−2535.
(55) Carrell, H. L.; Glusker, J. P.; Burger, V.; Manfre, F.; Tritsch, D.; Biellmann, J. F. *Proc. Natl. Acad. Sci. U. S.A.* **1989**, *86*, 4440−4.
(56) Fenn, T. D.; Ringe, D.; Petsko, G. A. *Biochemistry* **2004**, *43*, 6464−6474.
(57) Lavie, A.; Allen, K. N.; Petsko, G. A.; Ringe, D. *Biochemistry* **1994**, *33*, 5469−5480.
(58) Joy, R. A.; Arman, H.; Xiang, S.; Musie, G. T. *Inorg. Chim. Acta* **2013**, *394*, 220−228.
(59) Sanders-Loehr, J.; Wheeler, W. D.; Shiemke, A. K.; Averill, B. A.; Loehr, T. M. *J. Am. Chem. Soc.* **1989**, *111*, 8084−8093.
(60) Deacon, G. B.; Phillips, R. J. *Coord. Chem. Rev.* **1980**, *33*, 227−250.
(61) Zeleňák, V.; Vargová, Z.; Györyová, K. *Spectrochim. Acta, Part A* **2007**, *66*, 262−272.
(62) West, A. R. *Solid State Chemistry and Its Applications*; Wiley: Chichester, U.K., 1984; pp 553−560.
(63) Bain, G. A.; Berry, J. F. *J. Chem. Educ.* **2008**, *85*, 532.
(64) Barra, A. L.; Caneschi, A.; Gatteschi, D.; Sessoli, R. *J. Am. Chem. Soc.* **1995**, *117*, 8855−8856.
(65) Barra, A. L.; Debrunner, P.; Gatteschi, D.; Ch, E. S.; Sessoli, R. *Europhys. Lett.* **1996**, *35*, 133.
(66) Le Gall, F.; Fabrizi De Biani, F.; Caneschi, A.; Cinelli, P.; Cornia, A.; Fabretti, A. C.; Gatteschi, D. *Inorg. Chim. Acta* **1997**, *262*, 123−132.
(67) Panasci, A. F.; Ohlin, C. A.; Harley, S. J.; Casey, W. H. *Inorg. Chem.* **2012**, *51*, 6731−6738.
(68) Schmitt, W.; Anson, C. E.; Sessoli, R.; Van Veen, M.; Powell, A. K. *J. Inorg. Biochem.* **2002**, *91*, 173−189.
(69) Tan, X.-W.; Wang, B.-M.; Wang, Y.; Zhan, S.-Z. *Inorg. Chem. Commun.* **2010**, *13*, 1061−1063.
(70) Shin, J. W.; Bae, J. M.; Kim, C.; Min, K. S. *Dalton Trans.* **2014**, *43*, 3999−4008.
(71) Jameson, D. L.; Xie, C. L.; Hendrickson, D. N.; Potenza, J. A.; Schugar, H. J. *J. Am. Chem. Soc.* **1987**, *109*, 740−746.
(72) Tanase, T.; Inoue, C.; Ota, E.; Yano, S.; Takahashi, M.; Takeda, M. *Inorg. Chim. Acta* **2000**, *297*, 18−26.
(73) Kurtz, D. M. *Chem. Rev.* **1990**, *90*, 585−606.
(74) Bera, M.; Curtiss, A. B. S.; Musie, G. T.; Powell, D. R. *Inorg. Chem. Commun.* **2008**, *11*, 1033−1036.
(75) Bera, M.; Musie, G. T.; Powell, D. R. *Inorg. Chem. Commun.* **2010**, *13*, 1029−1031.
(76) Patra, A.; Sen, T. K.; Ghorai, A.; Musie, G. T.; Mandal, S. K.; Ghosh, U.; Bera, M. *Inorg. Chem.* **2013**, *52*, 2880−2890.
(77) Grimme, S. *Angew. Chem., Int. Ed.* **2008**, *47*, 3430−3434.
(78) Hunter, C. A.; Sanders, J. K. M. *J. Am. Chem. Soc.* **1990**, *112*, 5525−5534.
(79) Matthews, R. P.; Welton, T.; Hunt, P. A. *Phys. Chem. Chem. Phys.* **2014**, *16*, 3238−3253.
(80) Waters, M. L. *Curr. Opin. Chem. Biol.* **2002**, *6*, 736−741.
(81) Ferguson, A.; Mcgregor, J.; Parkin, A.; Murrie, M. *Dalton Trans.* **2008**, *2008*, 731−733.
(82) Murch, B. P.; Boyle, P. D.; Que, L. *J. Am. Chem. Soc.* **1985**, *107*, 6728−6729.
(83) Rose, N. J.; Drago, R. S. *J. Am. Chem. Soc.* **1959**, *81*, 6138−6141.
(84) Connors, K. A. *Binding Constants: The Measurement of Molecular Complex Stability*; Wiley: New York, 1987; p xiv, 411 p.
(85) Bera, M.; Patra, A. *Carbohydr. Res.* **2011**, *346*, 2075−2083.
(86) Coskuner, O.; Bergeron, D. E.; Rincon, L.; Hudgens, J. W.; Gonzalez, C. A. *J. Phys. Chem. A* **2008**, *112*, 2940−2947.
(87) Lawrence, G. D.; Mavi, A.; Meral, K. *Carbohydr. Res.* **2008**, *343*, 626−635.
(88) Rao, C. P.; Geetha, K.; Raghavan, M. S. S. *Biometals* **1994**, *7*, 25−29.
(89) Appendix 2: Dissociation Constants (pKa) of Common Sugars and Alcohols. In *Applications of Ion Chromatography for Pharmaceutical and Biological Products*; Bhattacharyya, L., Rohrer, J. S., Eds.; John Wiley & Sons, Inc.: Hoboken, NJ, 2012; pp 455−456.
(90) Hegetschweiler, K.; Hausherr-Primo, L.; Koppenol, W. H.; Gramlich, V.; Odier, L.; Meyer, W.; Winkler, H.; Trautwein, A. X. *Angew. Chem.* **1995**, *107*, 2421−2423.
(91) Burger, J.; Gack, C.; Klüfers, P. *Angew. Chem., Int. Ed.* **1996**, *34*, 2647−2649.
(92) *Spartan 10*; Wavefunction, Inc.: Irvine, CA, 2010.
(93) Lee, C.; Yang, W.; Parr, R. G. *Phys. Rev. B* **1988**, *37*, 785−789.
(94) Becke, A. D. *Phys. Rev. A* **1988**, *38*, 3098−3100.
(95) *CrystalClear User Manual*; Rigaku MSC/SSI Inc., Rigaku Corporation: Orem, UT.
(96) Higashi, T. *ASBCOR*; Rigaku Corporation: Tokyo, Japan, 1995.
(97) Sheldrick, G. M. *SHELX97. Program for the Solution of Crystal Structures*; University of Göttingen: Göttingen, Germany, 1997.
(98) Sheldrick, G. M. *SHELX97. Program for Crystal Structure Analysis*; University of Göttingen: Göttingen, Germany, 1997.